

Dusty winds: I. Self-similar solutions

Moshe Elitzur¹ and Željko Ivezić²

¹Department of Physics and Astronomy, University of Kentucky, Lexington, KY 40506-0055, USA; moshe@pa.uky.edu

²Department of Astrophysical Sciences, Princeton University, Princeton, NJ 08544-1001, USA; ivezic@astro.princeton.edu

Accepted May 15, 2001. Received May 6, 2001; in original form September 12, 2000

ABSTRACT

We address the dusty wind problem, from the point where dust formation has been completed and outward. Given grain properties, both radiative transfer and hydrodynamics components of the problem are fully defined by four additional input parameters. The wind radiative emission and the shape of its velocity profile are both independent of the actual magnitude of the velocity and are determined by just three dimensionless free parameters. Of the three, only one is always significant—for most of phase space the solution is described by a set of similarity functions of a single independent variable, which can be chosen as the overall optical depth at visual τ_V . The self-similarity implies general scaling relations among mass loss rate (\dot{M}), luminosity (L) and terminal velocity (v_∞). Systems with different \dot{M} , L and v_∞ but the same combination $\dot{M}/L^{3/4}$ necessarily have also the same $\dot{M}v_\infty/L$. For optically thin winds we find the exact analytic solution, including the effects of radiation pressure, gravitation and (sub- and supersonic) dust drift. For optically thick winds we present numerical results that cover the entire relevant range of optical depths, and summarize all correlations among the three global parameters in terms of τ_V . In all winds, $\dot{M} \propto v_\infty^3(1 + \tau_V)^{1.5}$ with a proportionality constant that depends only on grain properties. The optically thin end of this universal correlation, $\dot{M} \propto v_\infty^3$, has been verified in observations; even though the wind is driven by radiation pressure, the luminosity does not enter because of the dominant role of dust drift in this regime. The \dot{M} – L correlation is $\dot{M} \propto (L\tau_V)^{3/4}(1 + \tau_V)^{1.05}$. At a fixed luminosity, \dot{M} is *not* linearly proportional to τ_V , again because of dust drift. The velocity-luminosity correlation is $v_\infty \propto (L\tau_V)^{1/4}(1 + \tau_V)^{-0.465}$, explaining the narrow range of outflow velocities displayed by dusty winds. Eliminating τ_V produces $v_\infty^3 = A\dot{M}\left(1 + B\dot{M}^{4/3}/L\right)^{-1.5}$, where A and B are coefficients that contain the only dependence of this universal correlation on chemical composition. At a given L , the maximal velocity of a dusty wind is $v_{\max} \propto L^{1/4}$ attained at $\dot{M} \propto L^{3/4}$, with proportionality coefficients derived from A and B .

Key words: circumstellar matter — dust — infrared: stars — stars: AGB and post-AGB — stars: late-type — stars: winds, outflows

1 INTRODUCTION

Stars on the asymptotic giant branch (AGB) make a strong impact on the galactic environment. Stellar winds blown during this evolutionary phase are an important component of mass return into the interstellar medium and may account for a significant fraction of interstellar dust. These dusty winds reprocess the stellar radiation, shifting the spectral shape toward the infrared. There are good indications that they dominate the IR signature of normal elliptical galaxies (Knapp, Gunn & Wynn-Williams, 1992). In addition to

its obvious significance for the theory of stellar evolution, the study of AGB winds has important implications for the structure and evolution of galaxies.

Because of the reddening, dusty winds are best studied in the infrared. Since the observed radiation has undergone significant processing in the surrounding dust shell, interpretation of the observations necessitates detailed radiative transfer calculations. The complexity of these calculations is compounded by the fact that the wind driving force is radiation pressure on the grains; complete calculations require a solution of the coupled hydrodynamics and radiative

transfer problems. Traditionally these calculations involved a large number of input parameters that fall into two categories. The first one involves the dust properties; widely employed quantities include the dust abundance, grains size distribution, solid density, condensation temperature and absorption and scattering efficiencies. The second category involves global properties, including the stellar temperature T_* , luminosity $L = 10^4 L_4$ L $_{\odot}$, mass $M = M_0$ M $_{\odot}$ and the mass-loss rate $\dot{M} = 10^{-6} \dot{M}_{-6}$ M $_{\odot}$ yr $^{-1}$.

The large number of input quantities complicates modeling efforts, making it unclear what are the truly independent parameters and which properties can actually be determined from a given set of data. In a previous study we noted that the dusty wind problem possesses general scaling properties such that, for a given type of grains, both the dynamics and radiative transfer depend chiefly on a single parameter — the overall optical depth (Ivezić & Elitzur 1995, hereafter IE95). In a subsequent study we established in full rigor the scaling properties of the dust radiative transfer problem under the most general, arbitrary circumstances (Ivezić & Elitzur 1997, hereafter IE97). Here we extend rigorous scaling analysis to the other aspect of the dusty wind problem, the dynamics.

In scaling analysis the basic equations are reduced to the minimal number of free parameters that are truly independent of each other. By its nature, such analysis is driven by the underlying mathematics, and the proper free parameters are not necessarily convenient for handling the data. Attempting to make our presentation tractable we have separated it into two parts. The present paper discusses all the theoretical and mathematical aspects of the dusty wind problem. In a companion paper (Ivezić & Elitzur 2001, paper II hereafter) written as a stand-alone, the observational implications are discussed separately on their own. Readers mostly interested in practical applications may proceed directly to paper II.

2 UNDERLYING THEORY

2.1 Problem Overview

The complete description of a dusty wind should start at its origin, the stellar atmosphere. Beginning with a full atmospheric model, it should incorporate the processes that initiate the outflow and set the value of \dot{M} . These processes are yet to be identified with certainty, the most promising are stellar pulsation (e.g. Bowen 1989) and radiation pressure on the water molecules (e.g. Elitzur, Brown & Johnson 1989). Proper description of these processes should be followed by that for grain formation and growth, and subsequent wind dynamics.

An ambitious program attempting to incorporate as many aspects of this formidable task as possible has been conducted over the past few years, yielding models in qualitative agreement with observations (see Fleischer, Winters & Sedlmayr 1999 and Höfner 1999, and references therein). However, the complexity of this undertaking makes it difficult to assess the meaning of its successes. In spite of continuous progress, detailed understanding of atmospheric dynamics and grain formation is still far from complete. When involved models succeed in spite of the many uncertain in-

gredients they contain, it is not clear whether these ingredients were properly accounted for or are simply irrelevant to the final outcome.

Fortunately, the full problem splits naturally to two parts, as recognized long ago by Goldreich & Scoville (1976, GS hereafter). Once radiation pressure on the dust grains exceeds all other forces, the rapid acceleration to supersonic velocities produces complete decoupling from the earlier phases that contain all the major uncertainties. Subsequent stages of the outflow are independent of the details of dust formation—they depend only on the final properties of the grains, not on how these grains were produced; the supersonic phase would be exactly the same in two different outflows if they have the same mass-loss rate and grain properties even if the grains were produced by entirely different processes. Furthermore, these stages are controlled by processes that are much less dependent on detailed micro-physics, and are reasonably well understood. And since most observations probe only the supersonic phase, models devoted exclusively to this stage should reproduce the observable results while avoiding the pitfalls and uncertainties of dust formation and the wind initiation. For these reasons, the GS approach with its focus on the supersonic phase has been widely used in studies of the dusty wind problem (including recent ones by Netzer & Elitzur 1993, NE hereafter, and Habing, Tignon & Tielens 1994, HTT hereafter). This is the problem we address here.

2.1.1 Overall Plan

We consider a spherical wind in steady state (the steady-state assumption is adequate as long as the wind structure is not resolved in too fine details; see IE95). Our starting point is the radius r_1 beyond which the properties of individual dust grains do not change and radiation pressure is the dominant force on the envelope. When positions in the shell are specified in terms of the scaled radius $y = r/r_1$, the shell inner boundary is always at $y = 1$ and the actual magnitude of r_1 drops out of the problem. The equation of motion is $\rho dv/dt = \mathcal{F}$, where \mathcal{F} is the net outward radial force per unit volume, v is the gas velocity and $\rho = n_{\text{H}} m_{\text{p}}$ is its density (n_{H} is the number density of hydrogen nuclei and m_{p} is the proton mass). In steady-state $dt = dr/v$ and the equation becomes

$$\frac{dv^2}{dy} = 2a_{\mathcal{F}}r_1, \quad (1)$$

where $a_{\mathcal{F}} = \mathcal{F}/\rho$ is the acceleration associated with force \mathcal{F} . Since $a_{\mathcal{F}}r_1$ has dimensions of v^2 , any force can always be characterized by the velocity scale it introduces.

Winds of interest are highly supersonic, therefore the gas pressure gradient can be neglected (see also §5). The expansion is driven by radiation pressure on the dust grains and is opposed by the gravitational pull of the star. The dust and gas particles are coupled by the internal drag force. For each of these three force components we first derive the characteristic velocity scale and the dimensionless profile associated with its radial variation. With the resulting expressions we identify all the dimensionless free parameters and formulate the problem in terms of independent dimensionless variables, resulting in two coupled equations for the dynamics

	Carbon	Silicate
a (μm)	0.1	0.1
T_c (K)	800	800
Q_V	2.40	1.15
Q_*	.599	.114
Ψ_0	5.97	2.72

Table 1. Standard parameters for dust grains used in all numerical calculations. The efficiency factors are from Hanner 1988 for amorphous carbon, and Ossenkopf, Henning & Mathis 1992 for (the “warm” version of) silicate grains. The grain size a and sublimation temperature T_c are assumed. The lower part lists derived quantities: Q_V is the efficiency factor for absorption at visual; Q_* is the Planck average at the stellar temperature of the efficiency coefficient for radiation pressure (equation 4); Ψ_0 is defined in equation 41.

and radiative transfer. We proceed to solve the mathematical problem, and afterwards transform the dimensionless free parameters back into the physical variables that characterize the system. This procedure ensures that its outcome contains all the correlations that exist among the physical parameters of dusty winds.

Our presentation starts with a single type of dust grains, section 6 extends the discussion to mixtures of sizes and chemical compositions. The grain is specified by its size a , condensation temperature T_c and absorption and scattering efficiencies $Q_{\text{abs},\lambda}$ and $Q_{\text{sca},\lambda}$. We associate the radius r_1 with prompt dust formation so that $T_d(r_1) = T_c$. The mathematical problem does not contain any reference to r_1 , its actual magnitude enters only during the final transformation to physical quantities. We address this issue again in our summary in section 7. Table 1 lists the dust properties used in our numerical applications. Appendix A contains a glossary of all the relevant symbols.

2.2 Dynamics

We start with a discussion of the three force components controlling the supersonic phase, identifying in each case the characteristic velocity scale and the dimensionless profile of its radial variation. These physical processes have been discussed extensively in the literature, most recently by NE and HTT. We repeat the essential ingredients to establish the proper formalism and examine the various assumptions underlying the theory. We also offer a slightly improved expression for the dust drift velocity, accounting for the subsonic regime.

2.2.1 Radiation Pressure

The radiation pressure force per unit volume is

$$\mathcal{F}_{\text{rad}} = \frac{1}{c} n_d \pi a^2 \int Q_{\text{pr},\lambda} F_\lambda d\lambda. \quad (2)$$

Here Q_{pr} is the radiation pressure efficiency ($= Q_{\text{abs}} + Q_{\text{sca}}$, assuming isotropic scattering) and F_λ is the local radiative flux, comprised of the attenuated-stellar and diffuse contributions; note that the diffuse flux vanishes at r_1 (IE97). The

spectral matching between F_λ and the dust opacity varies in the wind because of the reddening of the radiation. This variation is conveniently described by the following radial profile, normalized to unity at $y = 1$:

$$\phi(y) = \frac{1}{Q_*} \int Q_{\text{pr},\lambda} \frac{F_\lambda(y)}{F(y)} d\lambda. \quad (3)$$

Here $F = \int F_\lambda d\lambda$ is the bolometric flux and

$$Q_* = \int Q_{\text{pr},\lambda} \frac{F_\lambda(1)}{F(1)} d\lambda = \frac{\pi}{\sigma T_*^4} \int Q_{\text{pr},\lambda} B_\lambda(T_*) d\lambda, \quad (4)$$

where B_λ is the Planck function. Table 1 lists the values of Q_* for our standard grains and $T_* = 2500$ K; the dependence on T_* is insignificant when this quantity is varied within its physical range. Because of the reddening of the radiation, the spectral matching tends to decrease with radial distance so that $\phi(y) \leq 1$.

The velocity scale associated with the radiation pressure force is defined via $v_p^2 = 2 r_1 \mathcal{F}_{\text{rad}}(r_1) / \rho(r_1)$. Introduce

$$\sigma_g = \pi a^2 \frac{n_d}{n_H} \Big|_c = 10^{-22} \sigma_{22} \text{ cm}^2, \quad (5)$$

the cross-section area per gas particle upon dust condensation. Then

$$v_p = \left(\frac{Q_* \sigma_g L}{2 \pi m_p c r_1} \right)^{1/2} = 111 \text{ km s}^{-1} \left(\frac{Q_* \sigma_{22} L_4}{r_{1,14}} \right)^{1/2}, \quad (6)$$

where $r_{1,14} = r_1 / 10^{14}$ cm. Ignoring momentarily the drag and gravity effects, the radiative force gives the equation of motion

$$\frac{dv^2}{dy} = \frac{v_p^2}{y^2} \phi(y). \quad (7)$$

When reddening is neglected too, $\phi = 1$ and the solution is simply

$$v^2 = v_T^2 + v_p^2 \left(1 - \frac{1}{y} \right). \quad (8)$$

Here we take as the starting point for the outflow velocity the isothermal sound speed

$$v_T = \left(\frac{k T_k}{m_{H_2}} \right)^{1/2} = 2.03 T_{k3}^{1/2} \text{ km s}^{-1} \quad (9)$$

where $T_k = T_{k3} \times 1000$ K is the kinetic temperature at $y = 1$ (not necessarily equal to the dust temperature at that point). In this approximation, first derived in GS, the outflow final velocity is $(v_T^2 + v_p^2)^{1/2} \simeq v_p$, since v_T is usually negligible. Typical values for the free parameters produce a velocity scale v_p considerably higher than observed outflow velocities, a problem noted by Castor (1981) as a serious shortcoming of dust-driven wind models. The effects of reddening, drift and gravity must supplement radiation pressure for a viable explanation.

2.2.2 Drag

Collisional coupling accelerates the gas particles and decelerates the dust. Gilman (1972) has shown that the dust-gas relative velocity reaches steady state within a distance $\ell \ll r_1$ and that the dust then fully mediates to the gas the radiation pressure force. In steady-state drift the drag force

can be eliminated and the separate equations of motion for the dust and gas combined into a single equation. HTT provide a useful discussion of this approach, which is the one taken here. Still, the dust drift has an important effect because the radiative acceleration is proportional to n_d/n_H , and separate mass conservation for the dust and the gas implies $n_d/n_H \propto v/v_d$; in spite of our assumption of prompt dust formation and no further formation or destruction, the dust abundance varies in the shell because of the difference between the dust and gas velocities.

In appendix B we derive a simple expression for the drift velocity, including both the subsonic and supersonic regimes. The drift effect introduces the independent velocity scale

$$v_m = \frac{Q_* L}{\dot{M} c} = 203 \text{ km s}^{-1} \frac{Q_* L_4}{\dot{M}_{-6}} \quad (10)$$

and the steady-state drift velocity is

$$v_{\text{rel}} = \frac{v_m v \phi}{v_T + \sqrt{v_m v \phi}} \quad (11)$$

(equation B4). The significance of subsonic drift is rapidly diminished with radial distance because v is increasing as the gas accelerates while v_T is decreasing as it cools down. The radial variation of v_T requires the gas temperature profile, a quantity that does not impact any other aspect of the flow and whose calculation contains large uncertainties. We avoid these uncertainties and use instead the initial v_T throughout the outflow. This slightly overestimates the overall impact of subsonic drift, producing a negligible error in an effect that is small to begin with.

The dust velocity is $v_d = v + v_{\text{rel}}$, therefore n_d/n_H varies in proportion to the dimensionless drift profile

$$\zeta(y) = \frac{v}{v_d} = \frac{v_T + \sqrt{v_m v \phi}}{v_T + v_m \phi + \sqrt{v_m v \phi}}. \quad (12)$$

Since $\pi a^2 n_d(y)/n_H(y) = \sigma_g \zeta(y)$ for $y \geq 1$, the force equation including the drift effect is

$$\frac{dv^2}{dy} = \frac{v_p^2}{y^2} \phi(y) \zeta(y). \quad (13)$$

Because of the drift, at $y = 1$ the radiative force is reduced by a factor $\zeta(1)$, a significant reduction when $v_m \gg v_T$. The reason is that the dust particles are produced at the velocity v_T with a certain abundance and the drift immediately dilutes that abundance within a distance $\ell \ll r_1$ so that n_d/n_H is diminished already at $y = 1$. In calculations that keep track separately of the dust and the gas, the two species start with the same velocity and this dilution is generated automatically (cf NE, HTT). Here we solve for only one component, the two species start with different velocities at $y = 1$ and the initial dilution must be inserted explicitly.

It is important to note that ζ is a monotonically increasing function of y (see figure 2 below). Therefore, the dust abundance is the smallest at $y = 1$ and increases from this minimum during the outflow. At the wind outer regions, n_d/n_H exceeds its initial value by the factor $\zeta(\infty)/\zeta(1)$.

2.2.3 Gravity

The gravitational pull introduces an independent velocity scale, the escape velocity at r_1

$$v_g = \left(\frac{2GM}{r_1} \right)^{1/2} = 15.2 \text{ km s}^{-1} \left(\frac{M_0}{r_{1,14}} \right)^{1/2}, \quad (14)$$

which is frequently entered in terms of the dimensionless ratio

$$\Gamma = \frac{\mathcal{F}_{\text{rad}}}{\mathcal{F}_{\text{grav}}} \Big|_{r_1} = \frac{v_p^2}{v_g^2} = \frac{Q_* \sigma_g L}{4\pi G M m_p c} = 45.8 Q_* \sigma_{22} \frac{L_4}{M_0}. \quad (15)$$

Gravity does not introduce any radial profile beyond its y^{-2} variation. Adding the gravitational effects, the equation of motion becomes

$$\frac{dv^2}{dy} = \frac{v_p^2}{y^2} \left[\phi(y) \zeta(y) - \frac{1}{\Gamma} \right]. \quad (16)$$

In the limit of negligible drift and reddening ($\zeta = \phi = 1$), the gravitational pull reduces the wind terminal velocity from v_p to $v_p(1 - 1/\Gamma)^{1/2}$, typically only $\sim 1\%$ effect.

This is the complete form of the equation of motion, including all the dynamical processes in the wind. The outflow is fully specified by the four independent velocity scales v_p , v_m , v_g and v_T , which is also the initial velocity $v(y = 1)$, and the reddening profile ϕ . This profile varies with the overall optical depth and is determined from an independent equation, the equation of radiative transfer.

2.3 Radiative Transfer

Because of the spherical symmetry, the radiative transfer equation requires as input only two additional quantities (IE97). One is the overall optical depth along a radial ray at one wavelength, which we take as visual

$$\tau_V = r_1 \sigma_V \int n_d dy; \quad (17)$$

the optical depth at every other wavelength is simply $\tau_V Q_\lambda / Q_V$, where Q_λ and Q_V are the absorption efficiencies at λ and visual, respectively. The other required input is the normalized radial profile of the dust density distribution

$$\eta(y) = \frac{n_d(y)}{\int_1^\infty n_d dy}. \quad (18)$$

Given these two quantities, the intensity $I_\lambda(y, \beta)$ of radiation propagating at angle β to the radius vector at distance y can be obtained from

$$\frac{dI_\lambda(y, \beta)}{d\tau_\lambda(y, \beta)} = S_\lambda - I_\lambda, \quad (19)$$

where

$$\tau_\lambda(y, \beta) = \tau_V \frac{Q_\lambda}{Q_V} \int_0^{y \cos \beta} \eta \left(\sqrt{z^2 + y^2 \sin^2 \beta} \right) dz. \quad (20)$$

In general, η and τ_V must be specified as independent input. Instead, here they are fully specified by the dynamics problem. With the assumption of no grain growth or sputtering after its prompt formation, mass conservation for the dust gives $n_d \propto 1/r^2 v_d \propto \zeta/y^2 v$ so that

$$\eta(y) = \frac{\zeta(y)}{y^2 v(y)} \left(\int_1^\infty \frac{\zeta}{y^2 v} dy \right)^{-1}. \quad (21)$$

Therefore η is not an independent input property, instead it is determined by the solution of the equation of motion. And straightforward manipulations show that

$$\tau_V = Q_V \frac{v_p^2}{2v_m} \int_1^\infty \frac{\zeta}{y^2 w} dy, \quad (22)$$

so τ_V , too, does not require the introduction of any additional independent input. The radiative transfer problem is fully specified by the parameters already introduced to formulate the equation of motion; it requires no additional input.

This completes the formulation of the dusty wind problem. The dynamics and radiative transfer problems are coupled through the reddening profile ϕ . The solution of the equation of motion obtained with a certain such profile determines a dust distribution η and an optical depth τ_V . The solution of the radiative transfer equation obtained with these η and τ_V as input properties must reproduce the reddening profile ϕ that was used in the equation of motion to derive them.

2.4 Scaling

Given grain properties and the spectral profile of the stellar radiation, the wind problem is fully specified by the four independent velocities v_p , v_m , v_g and v_T , which together form the complete input of the problem. Since an arbitrary velocity magnitude can always be scaled out, the mathematical model can be described in a dimensionless form which includes only three parameters. We choose v_m for this purpose because it results in a particularly simple equation of motion. Introduce

$$w = v/v_m, \quad \theta = v_T/v_m, \quad P = v_p/v_m. \quad (23)$$

The parameter P characterizes the ratio of radiation pressure to drift effects. It is very large when the drift becomes negligible and goes to zero when the drift dominates. The equation of motion (16) becomes

$$\frac{dw^2}{dy} = \frac{P^2}{y^2} \left(\phi \zeta - \frac{1}{\Gamma} \right), \quad \text{where } \zeta = \frac{\theta + \sqrt{w\phi}}{\theta + \phi + \sqrt{w\phi}} \quad (24)$$

and where ϕ is determined from the solution of the radiative transfer equation (19) in which the dust distribution and optical depth are

$$\begin{aligned} \eta(y) &= \frac{\zeta(y)}{y^2 w(y)} \left(\int_1^\infty \frac{\zeta}{y^2 w} dy \right)^{-1}, \\ \tau_V &= \frac{1}{2} Q_V P^2 \int_1^\infty \frac{\zeta}{y^2 w} dy. \end{aligned} \quad (25)$$

In this new form, the mathematical model is fully specified by the three dimensionless parameters P , Γ and θ , where the latter is also the initial value $\theta = w(y=1)$. The velocity must rise at the origin, and since $\phi(1) = 1$ the parameters are subject to the constraint

$$\Gamma \zeta(1) > 1, \quad \text{i.e. } (\Gamma - 1)(\theta + \sqrt{\theta}) > 1. \quad (26)$$

This liftoff condition ensures that radiation pressure, with proper accounting for the dust drift, can overcome the initial gravitational pull. It can be viewed as either a lower limit on Γ for a given θ or, given Γ , a lower limit on θ .

The dusty wind problem has been transformed into a set of two general mathematical equations — the equation of motion (24) and the radiative transfer equation (19) with the input properties from equation (25). Given the spectral

shapes of the stellar radiation and the dust absorption coefficient, these equations are fully prescribed by P , Γ and θ . Both the radiative transfer and the dynamics equations are solved without any reference to v_m or any other velocity scale. The velocity scale is an extraneous parameter, entirely arbitrary as far as the solution is concerned. *The wind radiative emission and the shape of its velocity profile are both independent of the actual magnitude of the velocity.* In the following discussion we show that the shape of $w(y)$ turns out to be a nearly universal function, independent of input parameters within their relevant range, and that the final velocity $w_\infty = w(y \rightarrow \infty)$ is for all practical purposes only a function of P .

3 SOLUTIONS

The complete solution involves two elements — dynamics and radiative transfer. The impact of the radiative transfer on the dynamics can be conveniently expressed in terms of the quantity Φ , defined via

$$\frac{w_\infty}{\Phi} = \int_\theta^{w_\infty} \frac{dw}{\phi}. \quad (27)$$

That is, Φ is the velocity-weighted harmonic average of the reddening profile ϕ . Combining equations 24 and 25, it is easy to show that

$$\frac{\tau_V}{Q_V} = \frac{w_\infty}{\Phi} + \frac{P^2}{2\Gamma} \int_1^\infty \frac{dy}{y^2 w \phi}. \quad (28)$$

Therefore, when gravity is negligible ($\Gamma \gg 1$) the optical depth and the terminal velocity obey the simple relation

$$w_\infty = \Phi \frac{\tau_V}{Q_V}. \quad (29)$$

In optically thin winds $\Phi = 1$ and $w_\infty = \tau_V/Q_V$. As reddening increases Φ decreases, the final velocity is affected by the radiative transfer and numerical computations are necessary.

We obtain numerical solutions for arbitrary optical depths with the code DUSTY (Ivezic, Nenkova & Elitzur, 1999). DUSTY solves the dusty wind problem through a full treatment of the radiation field, including scattering, absorption and emission by the dust, coupled to the hydrodynamics problem formulated above. Appendix D provides a description of the numerical procedure. We present now the solutions, starting with the optically thin regime where we found the exact analytic solution.

3.1 Negligible Reddening

When reddening is negligible, the flux spectral shape does not vary and $\phi = 1$ (see eq. 3). This is the situation in optically thin winds, and the detailed results presented in the next section show this to be the case when $\tau_V \lesssim 1$.^{*} Even though the optical depth at wavelengths shorter than visual already exceeds unity when $\tau_V = 1$ and the emerging

^{*} Another limit that in principle could give $\phi = 1$ involves grains so large that Q_λ is constant for all relevant wavelengths. This requires grain sizes in excess of $\sim 10 \mu\text{m}$, and seems of little relevance.

spectrum is affected by radiative transfer, the impact on the dynamics is minimal. The reason is that ϕ involves a spectral average, and the stellar radiation peaks at longer wavelengths.

The wind problem with $\phi = 1$ was called the ‘‘first simplified model’’ by HTT, who solved it numerically. Here we present the complete analytic solution for this case. Since ϕ is known, the equation of motion decouples from the radiative transfer problem and can be considered independently. Introduce

$$\delta = \frac{1}{\Gamma - 1}, \quad (30)$$

then equation 24 can be cast in the form

$$\left(1 + \frac{1 + \delta}{\sqrt{w} + \theta - \delta}\right) \frac{dw^2}{dy} = \frac{P^2}{1 + \delta} \frac{1}{y^2} \quad (31)$$

so that

$$w^2 - \theta^2 + 4(1 + \delta) \int \frac{x^3 dx}{x + \theta - \delta} = \frac{P^2}{1 + \delta} \left(1 - \frac{1}{y}\right). \quad (32)$$

The liftoff constraint (26) ensures that the denominator of the integrand never vanishes in physical solutions; it starts positive at the lower boundary and increases as x increases. The integration is standard, the result is

$$\begin{aligned} \frac{P^2}{1 + \delta} \left(1 - \frac{1}{y}\right) &= w^2 - \theta^2 + 4(1 + \delta) \left[\frac{1}{3} (w^{3/2} - \theta^{3/2}) \right. \\ &+ \frac{1}{2}(\delta - \theta)(w - \theta) \\ &+ (\delta - \theta)^2 (w^{1/2} - \theta^{1/2}) \\ &\left. + (\delta - \theta)^3 \ln \frac{\sqrt{w} + \theta - \delta}{\sqrt{\theta} + \theta - \delta} \right]. \end{aligned} \quad (33)$$

This is the complete solution for all dusty winds with $\tau_V < 1$, fully incorporating the effects of gravity and dust drift. Radiation reddening, which takes effect when $\tau_V > 1$, is the only ingredient missing from this analytic solution and preventing it from applicability for all winds. The GS solution (equation 8), the only previous analytic result, which neglected the effects of gravity and drift in addition to reddening, can be recovered inserting $\delta = 0$ and $P \gg 1$.

The solutions are meaningful only when describing winds in which v_∞/v_T is at least ~ 3 ; otherwise, the effects of gas pressure, which were neglected here, become significant and equation 24 loses its physical relevance. Therefore, we require $v_\infty/v_T = w_\infty/\theta > 3$. In addition, the liftoff condition implies that $\delta < \delta_{\max}$ where

$$\delta_{\max} = \sqrt{\theta} + \theta. \quad (34)$$

Figure 1 displays the dimensionless velocity profile as a function of distance y for a range of representative values of the three free parameters and demonstrates a remarkable property: Except for their role in determining the boundary of allowed phase space and controlling the wind properties near that boundary, δ and θ hardly matter; away from the boundary, the solution is controlled almost exclusively by the single parameter P . Part (a) of the figure shows the effect of varying δ when P and θ are held fixed. Each panel presents a representative value of P with a wind initial velocity $\theta = 0.03P$; this choice of θ ensures that the wind

velocity increase by a factor of ~ 10 –20 in each cases. The displayed values of δ cover the entire physical range for this parameter, from 0 to just below the singularity at δ_{\max} . In each panel, the solutions for $\delta/\delta_{\max} \leq \frac{1}{2}$ are rather similar to each other, those with $\delta/\delta_{\max} \leq \frac{1}{4}$ hardly distinguishable. All display a similar rapid rise within $y \lesssim 10$ toward a final, nearly the same velocity. The plots for $\delta/\delta_{\max} \geq 0.999$ stand out and show the quenching effect of gravity, which is discussed below (sec. 5.1).

The effect of θ on the solution when δ and P are held fixed are similarly shown in part (b) of the figure. In these panels $\delta = 0$. This value was chosen because it represents faithfully most non-quenched solutions while allowing the wind to start with arbitrarily small initial velocity, even zero. The values of θ for the displayed solutions are listed as fractions of θ_{\max} , the initial velocity that leads to $w_\infty/\theta = 3$ for the listed P . As is evident from the plots, the initial velocity is largely irrelevant. Starting from $\theta = 0$ or as much as $\frac{1}{2}\theta_{\max}$ yields practically the same results. The only discernible difference occurs at θ_{\max} , where the profile deviates from the common shape by no more than $\sim 10\%$.

The analytic solution defines w as an implicit function of y . In appendix C we derive explicit analytic expressions for w that provide adequate approximations in all regions of interest. An inspection of the solution shows that $P = 16/9$ is the transition between the drift-dominated regime at small P and negligible drift at large P . The velocity profiles in the two are

$$w = w_\infty \left(1 - \frac{1}{y}\right)^k, \quad k = \begin{cases} 2/3 & \text{for } P < 16/9 \\ 1/2 & \text{for } P > 16/9 \end{cases} \quad (35)$$

The expressions for w_∞ in the two regimes can be combined into the single form

$$w_\infty = P \left(\frac{P}{P + \frac{16}{9}}\right)^{1/3}. \quad (36)$$

The optical depth, needed for the radiative transfer problem which is solved independently in this case, is simply $\tau_V = Q_V w_\infty$ (see eq. 29). Appendix C provides the δ - and θ -corrections to these results, which show that the dependence on θ is confined to the very origin of the wind, $y - 1 \lesssim \theta/w_\infty$.

The last two expressions reproduce to within 30% the plots for all the non-quenched winds displayed in figure 1. They amplify our conclusion about the negligible role of both δ and θ away from the physical boundary and point to another remarkable property of the solution. Although the final velocity strongly depends on P , the shape of the velocity profile w/w_∞ does not. The only reference to P in this profile is in determining a transition to a slightly steeper profile shape at large P . The profile itself is independent of P in either regime and furthermore, the difference between the two shapes is not that large. These properties are evident from figure 1. Other than the numerical values on the vertical axes, it is hard to tell apart the plots in the different panels.

These results show that among the three independent input parameters, P is the only one to have a significant effect on any property of interest. Furthermore, even P affects mostly just the final velocity, it does not have a discernible effect on the shape of the velocity profile; *all optically thin winds share universal velocity and dust density profiles*.

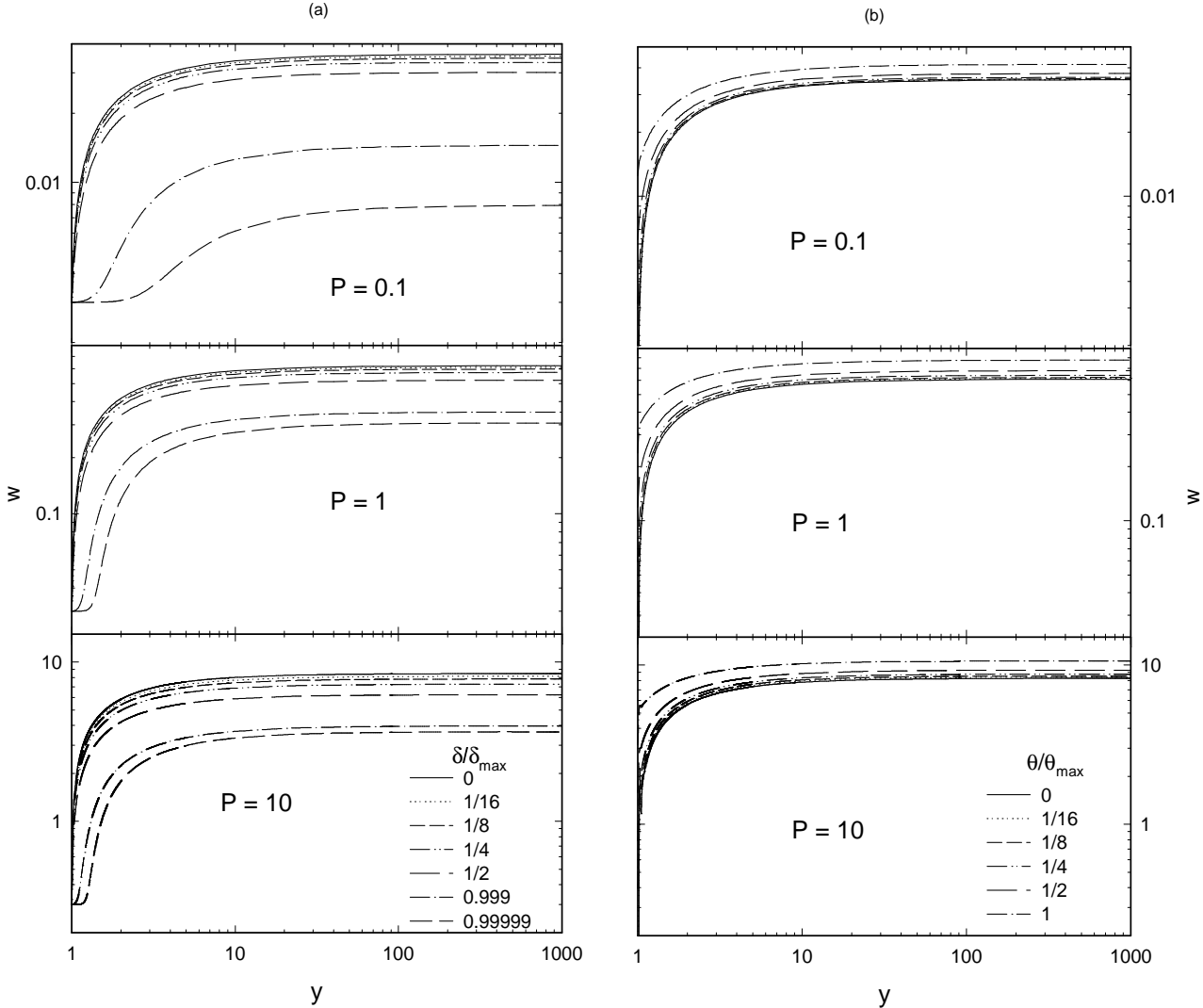


Figure 1. The complete solution (equation 33) for the velocity profiles of optically thin winds. (a) In each panel P has the indicated value and the initial velocity is $\theta = 0.03P$. The solutions are plotted for various values of δ , marked as fractions of the gravitational-quenching value δ_{\max} . Note the virtual δ -independence, except for the solutions asymptotically close to δ_{\max} . (b) Same as (a), only now θ varies and δ is fixed at 0. The values of θ are listed as fractions of θ_{\max} , the initial velocity that yields the smallest meaningful velocity increase $w_{\infty}/\theta = v_{\infty}/v_T = 3$. Note the complete θ -independence, except for the solution with $\theta = \theta_{\max}$.

3.2 Reddening Effects

The results for optically thin winds carry over to arbitrary optical depths, with profound implications for all winds. Reddening effects are controlled by the wind optical depth and density profile. For a given pair of δ and θ , consider a value of P sufficiently small that $\tau_V \ll 1$ so that reddening can be neglected; such a choice of P is virtually always possible. The velocity profile and τ_V are then uniquely determined by P (equations 35 and 36) and so is the radiative transfer problem. When P increases, τ_V increases too. The results of Appendix C show that

$$P = \frac{1}{Q_V} \left(1 + \frac{4}{3} Q_V^{1/2}\right)^{1/2} \quad (37)$$

yields $\tau_V = 1$; with our standard grains, the corresponding values are $P = 0.73$ for carbon and $P = 1.35$ for silicates. As P increases further the optical depth increases too and with it the impact of reddening, and that impact too is controlled

exclusively by P . Therefore, the parameter P controls all aspects of the problem. As concluded in IE95, away from its boundary and for most of phase space *the dusty wind problem is controlled by a single free parameter*. Since P , τ_V and w_{∞} are uniquely related to each other, either one can serve as that free parameter.

Figure 2 shows the radial variation of profiles of interest for various values of P . The models for $P = 0.1$, 1 and 10 repeat those presented in figure 1 but fully incorporate radiative transfer. Comparison of the corresponding plots in the two figures illustrates the impact of reddening. The bottom panel of figure 2 shows the reddening profile ϕ . Most of the reddening occurs close to wind origin. Reddening becomes significant at $P = 1$, and substantial at $P = 10$ and 100. Still it has only a minimal impact on the velocity profile; as is evident from the top panel, the dependence of the profile shape on P remains weak. We find that equation 35 remains an excellent approximation under all circumstances,

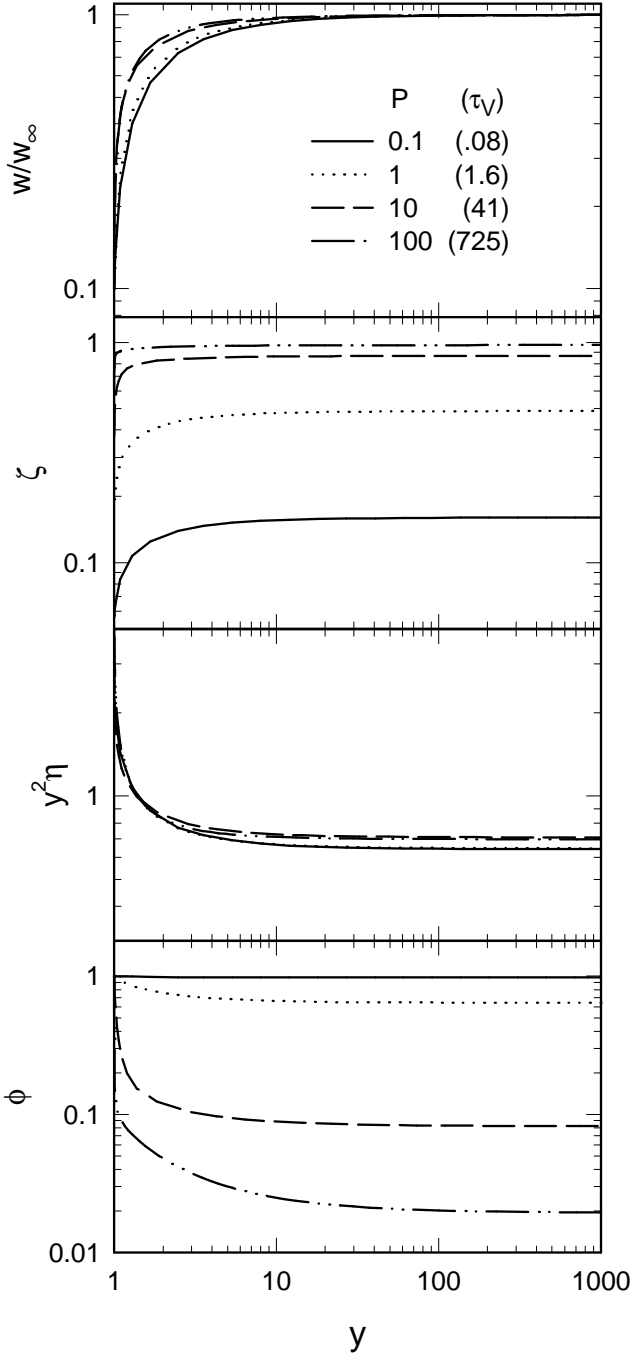


Figure 2. Radial profiles for quantities of interest at various values of P , as marked. The corresponding optical depths are shown in parentheses. All models have amorphous carbon grains, $\delta = 0$ and $w_\infty/\theta = 10$.

the effect of reddening merely decreases the exponent k from 0.5 to 0.4 at large P . The plots of ζ show that most of the drift variation, too, occurs close to the origin. At $y \gtrsim 2$ the dust and gas velocities maintain a constant ratio, which can be substantial when P is small; at $P = 0.1$ the final velocity of the dust grains exceeds that of the gas particles by more than factor 6. The velocity and drift profiles combine to determine the dust density profile η (see eq. 25). The figure

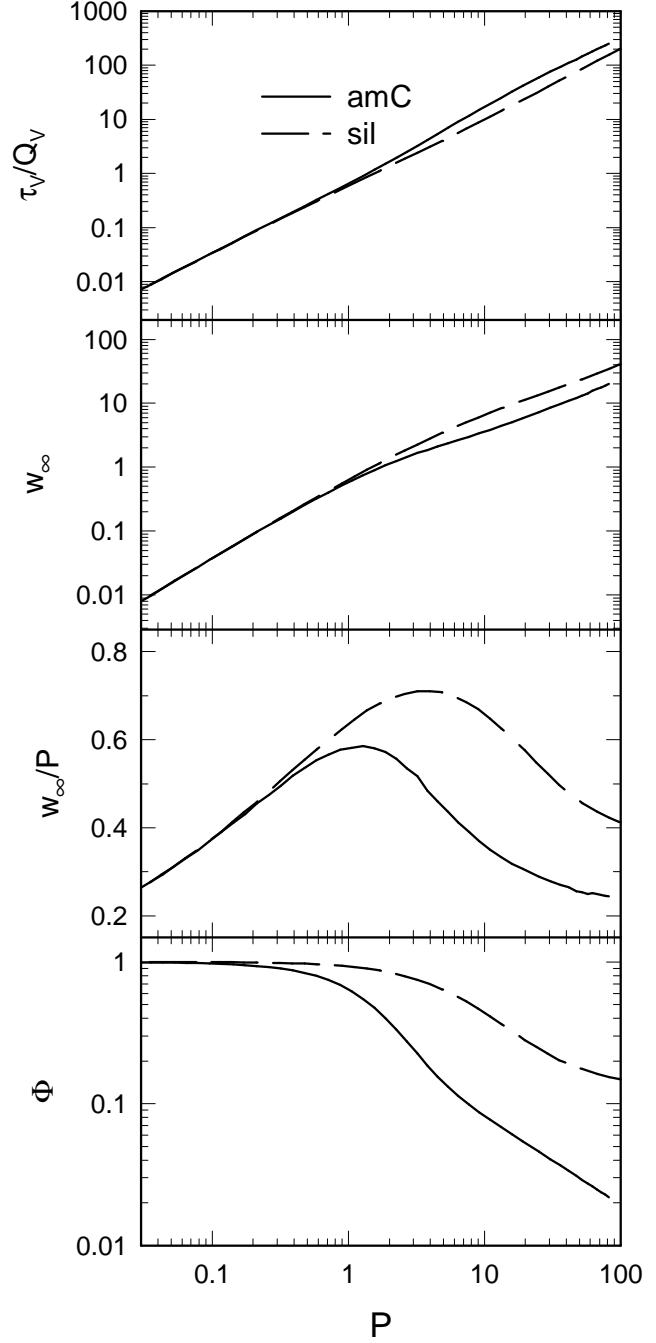


Figure 3. Variation with P of various quantities of interest.

Figure presents the function $y^2\eta$, removing the common radial divergence factor $1/y^2$.

The plots present the full solutions of the dynamics problem coupled with radiative transfer for carbon grains. The results for silicate grains are essentially the same, extending the conclusion reached in the optically thin limit to all cases: *all radiatively driven dusty winds share nearly identical velocity and dust density profiles*.

Figure 3 presents the dependence of τ_v/Q_v ($= w_\infty/\Phi$) and final velocity w_∞ on P . The bottom panel shows the reddening indicator Φ . As long as $\Phi = 1$, reddening is negligible, the analytic solution (33) holds and the grain prop-

erties are irrelevant. Indeed, all quantities are the same for carbon and silicate dust in that regime. The grain composition matters only when reddening affects the dynamics. The figure shows that Φ begins to decrease, indicating that reddening becomes significant, at a value of P corresponding to $\tau_V \simeq 1$; the actual value is controlled by Q_V (equation 37), it is larger for silicate because of its smaller Q_V . As noted before, the optical depth at wavelengths shorter than visual already exceeds unity when $\tau_V = 1$, but that spectral region has little impact on the dynamics.

Appendix B shows that the analytic approximation in equation 36 can be extended to include reddening effects,

$$w_\infty = P\sqrt{\Phi} \left(\frac{P}{P + \frac{16}{9}\sqrt{\Phi}} \right)^{1/3}. \quad (38)$$

This expression provides an excellent approximation for the numerical results presented in figure 3; the deviations are less than 10% for silicate grains, 30% for carbon. In addition to w_∞ , the figure displays also $w_\infty/P = v_\infty/v_p$. As discussed in §2, the simplest application of radiation pressure gives the GS result $v_\infty = v_p$, i.e. $w_\infty/P = 1$. The figure shows that the actual solution has a substantially different behavior — w_∞/P is neither constant, nor does it reach unity. Instead, it increases in proportion to $P^{1/3}$ at $P \lesssim 1$, because of the drift, and decreases in proportion to $\Phi^{1/2}$ at $P \gtrsim 1$, because of the reddening. Its maximum, reached around $P \sim 1$, is larger for silicate because it requires larger P for reddening to become significant. Drift and reddening play a crucial role in the behavior of w_∞/P . The maximum reached by this function translates to a maximum velocity for dusty winds, discussed in the next section.

4 OBSERVABLE CORRELATIONS

Contact with observations is made by transforming the mathematical problem back into physical quantities. Except for regions close to the boundary of phase space (see §5), the wind problem is fully controlled by the parameter P and its solution determines the corresponding w_∞ . Both quantities will now be expressed in terms of physical parameters.

The main scaling variable is

$$P = 0.546 \dot{M}_{-6} \left(\frac{\sigma_{22}}{Q_* L_4 r_{1,14}} \right)^{1/2} \quad (39)$$

(see equation 23). This expression does not determine P explicitly because P enters indirectly also on its right hand side. The dust condensation condition $T(r_1) = T_c$ determines r_1 as (IE97)

$$r_1 = \left(\frac{L\Psi}{16\pi\sigma T_c^4} \right)^{1/2} = 1.16 \times 10^{14} \frac{L_4^{1/2} \Psi^{1/2}}{T_{c3}^2} \text{ cm}. \quad (40)$$

Here $T_{c3} = T_c/(1000 \text{ K})$ and Ψ is a dimensionless function determined by the radiative transfer, similar to the reddening profile, and thus dependent on P . Optically thin winds have $\Psi = \Psi_0$ where

$$\Psi_0 = \frac{Q_P(T_*)}{Q_P(T_c)}. \quad (41)$$

Here $Q_P(T)$ is the Planck average of the absorption efficiency, similar to the average of the radiation pressure efficiency that defines Q_* (equation 4); Table 1 lists Ψ_0 for

our standard grains. As P increases, the wind becomes optically thick and Ψ increases too. In IE97 we present the variation of Ψ/Ψ_0 with optical depth and show that it is well approximated by the analytic expression

$$\frac{\Psi}{\Psi_0} = 1 + 3 \frac{\tau_V}{Q_V} Q_P(T_c) \bar{\phi} \quad (42)$$

where

$$\bar{\phi} = \int \phi(y) \eta(y) \frac{dy}{y^2}$$

(see figure 1 and equation B7 in IE97)[†]. Just as Φ is the velocity-weighted harmonic average of the reddening profile, $\bar{\phi}$ is its standard average, weighted by η/y^2 .

For most of the relevant region of phase space, P fully controls the solution of the dusty wind problem. Since Ψ is part of that solution, it too depends only on P . Therefore, the combination of equations 39 and 40 results in

$$\frac{\dot{M}_{-6}}{L_4^{3/4}} = 1.98 \frac{Q_*^{1/2}}{\sigma_{22}^{1/2} T_{c3}} P \Psi^{1/4}, \quad (43)$$

a one-to-one correspondence between $\dot{M}/L^{3/4}$ and P . This correspondence involves the function $P\Psi^{1/4}$, which is fully determined from the solution of the mathematical wind problem. The proportionality constant involves the individual grain properties Q_* and T_c which are part of the problem specification, and σ_{22} which is not. The dust abundance, necessary for specifying σ_{22} , has no effect on the wind solution; only the proportionality constant is modified when this abundance is varied, the function $P\Psi^{1/4}$ remains the same.

This result shows that for any dusty wind, the combination $\dot{M}/L^{3/4}$ can be determined directly from the shape of the spectral energy distribution: the wind IR signature is fully controlled by the parameter P , therefore comparing the observations with a bank of solutions determines the value of P and equation 43 fixes $\dot{M}/L^{3/4}$. We may expect all C-rich stars to have dust with roughly similar abundance and individual grain properties, so that they have the same proportionality constant and functional dependence $\Psi(P)$; likewise for O-rich stars. In that case, each family defines a unique correspondence between $\dot{M}/L^{3/4}$ and P . And since the parameter P fully controls the IR signature, stars that have different \dot{M} and L but the same $\dot{M}/L^{3/4}$ are indistinguishable by their IR emission because they also have the same P .

The solution of the wind problem also determines w_∞ , another unique function of P . Therefore, the relation $v_\infty/v_m = w_\infty$ gives another one-to-one correspondence between P and an independent combination of physical quantities

$$\frac{\dot{M} v_\infty}{L} = \frac{1}{c} Q_* w_\infty. \quad (44)$$

Since this correspondence does not involve σ_{22} , it is independent of the dust abundance and depends only on individual grain properties. Systems with different \dot{M} , L and v_∞ but the same $\dot{M}/L^{3/4}$ necessarily have also the same $\dot{M}v_\infty/L$.

[†] Since scattering is neglected in the IE97 analytic solution, the difference between Q_* and $Q_P(T_*)$ is ignored in the approximations here (but not in the numerical calculations).

because each combination uniquely determines the parameter P of the system.

The complete description of the wind problem involves four velocity scales, two of which (v_T and v_g) do not count whenever Γ and θ can be ignored. For most of phase space the problem is fully specified by the velocities v_p and v_m , and its solution determines v_∞ . The two ratios formed out of these three velocities are all the independent dimensionless combinations of physical parameters to determine the mathematical wind model and its solution. Since this solution fully specifies the wind IR signature, $\dot{M}/L^{3/4}$ and $\dot{M}v_\infty/L$ are the only combinations of global parameters that can be determined from IR observations, even the most detailed ones. When the velocity is additionally measured in molecular line observations so that both P and v_∞ are known, the two combinations in equations 43 and 44 can be used to determine also L and \dot{M} individually. The relevant correlations are

$$\frac{v_\infty}{L^{1/4}} \propto \frac{w_\infty}{P\Psi^{1/4}}, \quad \frac{v_\infty^3}{\dot{M}} \propto \frac{w_\infty^3}{P^4\Psi}, \quad (45)$$

whose constants of proportionality can be trivially derived. Only two of the last four combinations that relate \dot{M} , L and v_∞ to the solution are independent; any two of them can be derived from the other two.

4.1 Similarity Relations

While P is the natural independent variable of the mathematical problem, its physical interpretation is only indirect. Modeling of IR observations directly determines τ_V , not P . Therefore, we now express all results in terms of τ_V by performing a straightforward change of variables. The relation between τ_V and P is non-linear, starting from $P \propto \tau_V^{3/4}$ in the optically-thin regime and switching to a more complex dependence when reddening becomes significant. We introduce the τ_V - P transformation function Θ through

$$P = \frac{2}{\sqrt{3}} \left(\frac{\tau_V}{Q_V} \right)^{3/4} \Theta \quad (46)$$

so that $\Theta = 1$ when $\tau_V < 1$. At larger optical depths, Θ can only be determined from the numerical solution. The analytic expression

$$\Theta^2 \simeq \left[1 + \frac{3}{4} (\tau_V/Q_V)^{1/2} \right] \Phi, \quad (47)$$

obtained from equation C12, provides a useful approximation for the numerical results at all optical depths. With the τ_V - P transformation, equation 43 becomes

$$\frac{\dot{M}_{-6}}{L_4^{3/4}} = c_1 \tau_V^{3/4} K_1(\tau_V), \quad (48)$$

where

$$K_1 = \left(\frac{\Psi}{\Psi_0} \right)^{1/4} \Theta, \quad c_1 = 2.28 \frac{Q_*^{1/2} \Psi_0^{1/4}}{Q_V^{3/4} \sigma_{22}^{1/2} T_{c3}}.$$

From its definition $K_1 = 1$ when $\tau_V < 1$, therefore $\dot{M}_{-6} = c_1 (L_4 \tau_V)^{3/4}$ in all optically thin winds. As the optical depth increases, K_1 introduces the reddening correction to this relation. This correction, purely a function of τ_V , is shown in the top panel of figure 4.

The transformation of the other independent correlation from P to τ_V is considerably simpler. Thanks to equation 29, which holds for all winds when gravity is negligible, equation 44 can be cast similarly in the form

$$\frac{\dot{M}v_\infty}{L} = \frac{1}{c} (Q_*/Q_V) \tau_V K_2(\tau_V), \quad (49)$$

where $K_2 = \Phi$. The function K_2 , shown in the second panel of figure 4, contains the reddening corrections to the optically thin correlation, similar to the previous result. Since $K_2 = \Phi$, it is the same function as shown in figure 3, only plotted against the independent variable τ_V instead of P .

This completes the transformation from P to τ_V of the two independent correlations. In both, the luminosity does not enter independently, only through the product $L\tau_V$. In the case of equation 49 this is a direct consequence of the structure of the equation of motion, which gives $v_\infty = v_m w_\infty = v_m \tau_V (\Phi/Q_V)$. The combination $L\tau_V$ emerges here as a “kinematic” result irrespective of the explicit expression for the drift function. In the case of equation 48, on the other hand, this combination is a direct consequence of the specific functional form of ζ . With these two results, the correlations in eq. 45 become similarly

$$\frac{v_1}{L_4^{1/4}} = c_3 \tau_V^{1/4} K_3(\tau_V), \quad \frac{v_1^3}{\dot{M}_{-6}} = c_4 K_4(\tau_V) \quad (50)$$

where $K_3 = K_2/K_1$ and $K_4 = K_2^3/K_1^4$. The associated proportionality constants are

$$c_3 = 88.9 T_{c3} (Q_* \sigma_{22})^{1/2} (Q_V \Psi_0)^{-1/4} \\ c_4 = 3.08 \times 10^5 T_{c3}^4 Q_* \sigma_{22}^2 \Psi_0^{-1}. \quad (51)$$

Since L enters only in the form $L\tau_V$, the combination that eliminates L eliminates also τ_V from its optically thin regime. The reddening correction functions K_3 and K_4 are shown in the two bottom panels of figure 4.

At small τ_V the grain properties are irrelevant and the similarity K -functions are unity for both silicate and carbon dust. As τ_V increases the curves for the two species diverge, reflecting their different optical properties. However, figure 4 shows that the differences are quite moderate in all four cases. They are most noticeable in K_1 and K_2 , where the relative differences from the mean never exceed $\sim 25\%$. It is also important to note that the displayed range of τ_V greatly exceeds the observed range since cases of $\tau_V \gtrsim 10$ are rare. The differences are greatly reduced in the ratio function K_3 ($= K_2/K_1$) and practically disappear in K_4 . This function is essentially the same (within a few percent) for both silicate and carbon grains at all optical depths, an agreement maintained over many orders of magnitude. Evidently, K_4 is independent of chemical composition.

The universality of K_4 is no accident. From the analytic approximations for Ψ (eq. 42) and Θ (eq. 47), at large optical depths $\tau_V^2 K_4 \propto \Phi/\bar{\phi}$; that is, apart from the explicit dependence on τ_V , the variation of K_4 comes from the ratio of two averages of the reddening profile, one (Φ) strongly weighted toward the outer part of the shell the other ($\bar{\phi}$) toward the inner part. Although Φ and $\bar{\phi}$ are different for grains with different optical properties, their ratio is controlled by the shapes of the density and velocity profiles — which are universal, as shown above. As a result, the functional dependence of K_4 on τ_V is the same for all grains

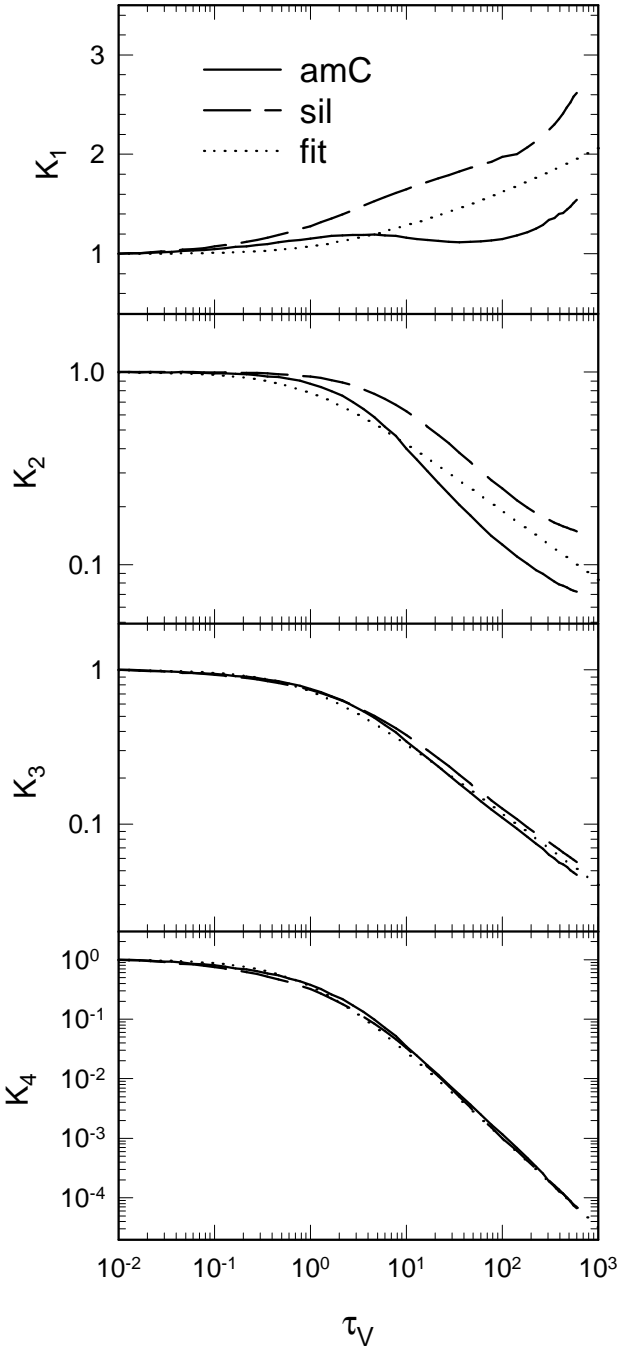


Figure 4. The reddening corrections in the scaling relations that summarize the physical contents of the solution (equations 48–50). Note the linear scale in the plot of K_1 . The full and dashed lines show the results of detailed numerical calculations for carbon and silicate grains, respectively. The dotted-line in the panel for K_i ($i = 1 \dots 4$) plots the function $1/(1+\tau_V)^{\alpha_i}$ where $\alpha_1 = -0.05$, $\alpha_2 = 0.36$, $\alpha_3 = 0.465$ and $\alpha_4 = 1.5$.

when $\tau_V \gg 1$ in addition to $\tau_V < 1$. This does not yet guarantee a universal profile because the transition between the two regimes could depend on the grain parameters. Indeed, the plot of $\Phi (= K_2)$ shows that the large- τ_V decline of this function is delayed for silicate in comparison with carbon dust. As explained in the discussion of figure 3, the onset

of reddening requires a larger τ_V for silicate because of its smaller Q_V . But the behavior of the factor $1 + \frac{3}{4}(\tau_V/Q_V)^{1/2}$ in Θ (eq. 47) is precisely the opposite since its large- τ_V behavior starts earlier when Q_V is smaller. The two effects offset each other, producing a universal shape.

The simple analytic expression $(1+\tau_V)^{-1.5}$ fits the function K_4 to within 20% over a variation range covering more than four orders of magnitude, providing the nearly perfect fit evident in figure 4. Therefore, dusty winds obey the condition

$$\frac{v_1^3}{\dot{M}_6} (1 + \tau_V)^{1.5} = c_4. \quad (52)$$

This result provides a complete separation of the system global parameters from the grain parameters. The combination of v_∞ , \dot{M} and τ_V on the left hand side is always constant, its magnitude is determined purely by the dust properties. This expression makes it evident again that the optically thin regime corresponds to $\tau_V < 1$.

As is evident from figure 4, K_3 too is nearly the same for carbon and silicate grains. The reason is that $K_3 = (K_2 K_4)^{1/4}$ and the only difference between the two species comes from their K_2 profiles, which enter only in the fourth root. The single analytic expression $(1 + \tau_V)^{-0.465}$ provides an excellent fit for both silicate and carbon grains, leading to the independent correlation

$$v_1 = c_3 (L_4 \tau_V)^{1/4} (1 + \tau_V)^{-0.465}. \quad (53)$$

This result can explain the narrow range of velocities observed in dusty winds. The dependence of velocity on τ_V at fixed luminosity and grain properties is shown in figure 5. This function reaches a maximum of 0.73 at $\tau_V = 1.3$, therefore the largest velocity a dusty wind can have is

$$v_{\max} = 0.73 c_3 L_4^{1/4} \text{ km s}^{-1}. \quad (54)$$

Figure 5 shows that the deviations from this maximum are no more than a factor of ~ 2 when τ_V is varied in either direction by two orders of magnitude. The dependence of velocity on luminosity is only $L^{1/4}$, and since L_4 is typically $\sim 0.3\text{--}20$ it introduces a similarly small variation. Finally, even the dependence on grain properties is weak, as is evident from the expression for c_3 (eq. 51). The only grain parameter that enters linearly is the condensation temperature, and its dispersion is expected to be small.

Since only two of the K -functions are independent, the universal fits for K_3 and K_4 can be used to produce grain-independent approximations also for K_1 and K_2 . Figure 4 shows that the single function $K_3^3/K_4 = (1 + \tau_V)^{0.105}$ provides an adequate fit for K_1 of both silicate and carbon dust, always within 30% of the detailed results[†]. This expression gives

$$\dot{M}_6 = c_1 (L_4 \tau_V)^{3/4} (1 + \tau_V)^{0.105}. \quad (55)$$

Since $\tau_V = 1.3$ gives the largest possible velocity at a given L , the corresponding mass loss rate is

$$\dot{M}_6(v_{\max}) = 1.33 c_1 L_4^{3/4}. \quad (56)$$

[†] Higher accuracy, when desired, can be obtained by replacing the common index 0.105 with 0.05 for amorphous carbon and 0.15 for silicate grains.

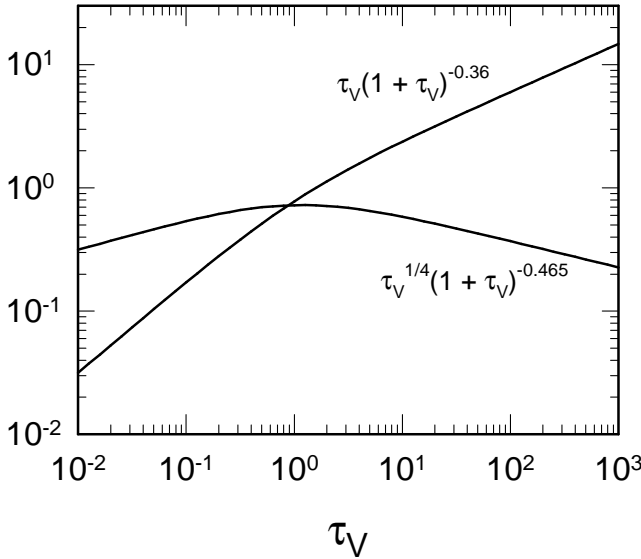


Figure 5. The τ_V -variation of the correlations 53 and 57.

A common practice in analysis of observations is to deduce the optical depth from spectral data and derive \dot{M} from τ_V (e.g., Jura 1991). This procedure is predicated on the assumption of a linear relationship between \dot{M} and τ_V , and our result shows that this assumption is not quite right. At a fixed luminosity, \dot{M} is proportional to $\tau_V^{3/4}$ in the optically thin regime and to $\tau_V^{0.86}$ at large τ_V . The expectation of a linear relationship between \dot{M} and τ_V is not met because of the dust drift, since $\tau_V/\dot{M} \propto \int (\zeta/y^2 v) dy$. The relationship would be linear if ζ were 1 everywhere, but figure 2 shows that this is never the case. The deviations from unity are large at small τ_V , where the drift is most prominent, decreasing as τ_V increases.

Finally, figure 4 shows that the universal profile $K_3^4/K_4 = (1+\tau_V)^{-0.36}$ again describes reasonably the actual K_2 of both grains, so that

$$\dot{M}v_\infty = \frac{L}{c} (Q_*/Q_V) \tau_V (1 + \tau_V)^{-0.36} \quad (57)$$

The relation $\dot{M}v_\infty \leq L/c$ has often been used as a physical bound on radiatively driven winds, even though the mistake in this application when $\tau_V > 1$ has been pointed out repeatedly. In IE95 we show that the proper form of momentum conservation is $\dot{M}v_\infty = \tau_F L/c$ where τ_F is the flux-averaged optical depth, so now we have found the explicit expression

$$\tau_F = (Q_*/Q_V) \tau_V (1 + \tau_V)^{-0.36}. \quad (58)$$

The τ_V -variation of this function is shown in figure 5. It increases linearly at small τ_V , reaches unity at $\tau_V = 1.6$ and switches to $\tau_V^{0.64}$ thereafter. The ratio Q_*/Q_V is 0.1 for silicate and 0.25 for carbon (see Table 1).

For every pair among \dot{M} , L and v_∞ , equations (52), (53) and (55) list the correlation in term of optical depth. When detailed IR data are not available and τ_V cannot be determined, it can be bypassed by correlating the pairs directly against each other. Since only two of the three relations are independent, there is only one such combination. Equation 55 is the most suitable for eliminating τ_V because K_1 varies the least among the four K -functions. In fact, the crude ap-

proximation $K_1 \simeq 1$ introduces an error of less than 50% for $\tau_V \lesssim 10$. With this approximation, $\tau_V \propto \dot{M}^{4/3}/L$. Inserting this result in equation 52 yields

$$v_1^3 = A \dot{M}_{-6} \left(1 + B \frac{\dot{M}_{-6}^{4/3}}{L_4} \right)^{-1.5} \quad (59)$$

where $A = c_4$ and $B = c_1^{-4/3}$. This universal correlation summarizes our solution for all dusty winds away from the boundaries of phase space. The error in this result, introduced by the approximation $K_1 = 1$, is less than 50% when $\tau_V \lesssim 10$. When the observational accuracy warrants higher precision, corrections can be readily derived.

This completes the similarity solution of the dusty wind problem. Our results amplify the conclusion of IE95, taking it a step further: The solution is fully characterized by optical depth. The relations among global parameters \dot{M} , L and v_∞ involve universal similarity functions of τ_V , independent of chemical composition. The grain properties enter only in the proportionality constants of the similarity relations. We derived the similarity functions from solutions for carbon and silicate grains, whose absorption efficiencies are widely different. Since dust spectral features have a negligible effect on overall reddening corrections, these functions should describe all interstellar grains with reasonable properties. It is gratifying that in spite of its great complexity, the dusty wind problem can afford such a simple, explicit solution.

4.2 Young's Correlation

Young (1995) conducted a survey of nearby Mira variables with low mass-loss rates. He finds a clear, strong correlation between outflow velocity and mass-loss rate, but independent of luminosity. The correlation can be parametrized as $M \propto v_\infty^\alpha$, with $\alpha = 3.35$. Subsequent observations by Knapp et al (1998) corroborate Young's results and find $\alpha = 2$, although the scatter in their data is consistent with values as large as 3. Remarkably, even though the wind is driven by radiation pressure, its velocity is independent of luminosity.

From equation 52 (or 59), at small optical depths our solution gives $\dot{M} \propto v_\infty^3$ independent of luminosity, explaining the observational findings. The implied $\alpha = 3$ is consistent with all observational results within their errors. This result reflects the central role of drift at small mass loss rates. When the drift dominates, $\zeta \simeq w^{1/2} \propto (\dot{M}v/L)^{1/2}$. Neglecting gravity and reverting to physical variables, the equation of motion (13) becomes

$$\frac{dv^2}{dr} \propto \frac{(\dot{M}Lv)^{1/2}}{r^2} \quad (60)$$

where the proportionality constant contains the grain properties. The solution gives $v_\infty^{3/2} \propto (\dot{M}L)^{1/2}/r_1$. And since r_1 is proportional to $L^{1/2}$ (eq. 40), the dependence on luminosity cancels out. If not for the particular L -dependencies of r_1 and the drift, this would not have happened.

The observed correlation, in particular its luminosity independence, directly reflects the specific dependence of the drag force on \dot{M} , L and v . Other forms for the force would produce different correlations. For example, when the drift is neglected, the combination $(\dot{M}Lv)^{1/2}$ is replaced by L , leading to the GS result $v_\infty = v_p \propto (L/r_1)^{1/2}$ (eq. 6). Together with $r_1 \propto L^{1/2}$ this yields $v_\infty^4 \propto L$, as first noted by

Jura (1984). This prediction of a correlation between velocity and luminosity independent of mass-loss rate is in strong conflict with the observations. One could formally eliminate the luminosity with the aid of the momentum flux conservation $Mv_\infty = \tau_F L/c$ (see eq. 57 and subsequent discussion) to re-write this result as $\dot{M} \propto \tau_F v_\infty^3$. While this bears superficial resemblance to Young's correlation, the observational result emerges only if the variation of τ_F with L and \dot{M} is ignored. By contrast, at $\tau_V < 1$ equations 55 and 58 together give $\tau_F \propto \tau_V \propto \dot{M}^{4/3}/L$.

Young's correlation is a direct reflection of the basic physics ingredients that went into the model. It demonstrates the importance of drift in dusty winds and provides strong support for its underlying theory.

5 PHYSICAL DOMAIN

A global property not considered thus far is the stellar mass. This quantity does not enter into the definition of the parameter P and thus cannot be determined in general. The mass only affects Γ (see equation 15), a quantity that can vary by orders of magnitude without a discernible effect on any observed property. However, Γ does play an important role in determining the parameter range corresponding to actual winds.

The equation of motion (24) has many mathematical solutions but not all of them are physically relevant. By example, consider the analytic solution for optically thin winds (equation 33), whose logarithmic term becomes singular when $\delta = \delta_{\max}$ (see equation 34). The singularity is avoided whenever the numerator and denominator are finite and have the same sign. Both cases are mathematically acceptable but the negative sign is physically meaningless. Such solutions violate the liftoff condition (equation 26) and the only transition from one set of solutions to the other is through the singularity.

At the outset, P , Γ and θ must be positive. Further, all winds must obey the liftoff condition, which involves only two out of the three input parameters. This condition ensures liftoff under all circumstances but it does not automatically guarantee a meaningful outcome. The formal solution of equation 24 gives

$$w_\infty^2 = \theta^2 + P^2 \left(\int_1^\infty \phi \zeta \frac{dy}{y^2} - \frac{1}{\Gamma} \right). \quad (61)$$

Obviously, in physical solutions the final velocity must exceed the initial velocity and we further require $v_\infty/v_T \gtrsim 3$ (see §3.1). Because $\phi \leq 1$ and $\zeta < 1$, $\int_1^\infty (\phi \zeta / y^2) dy < 1$ and

$$P^2 > \theta^2 \frac{\Gamma}{\Gamma - 1} \left(\frac{v_\infty^2}{v_T^2} - 1 \right). \quad (62)$$

The three parameters of every dusty wind whose velocity increases by the ratio v_∞/v_T must also obey this constraint.

5.1 Gravitational Quenching

The wind acceleration is positive as long as $\Gamma \phi \zeta > 1$ (eq. 24). Negative acceleration, leading to wind quenching, can be caused by increasing either the gravitational pull (smaller

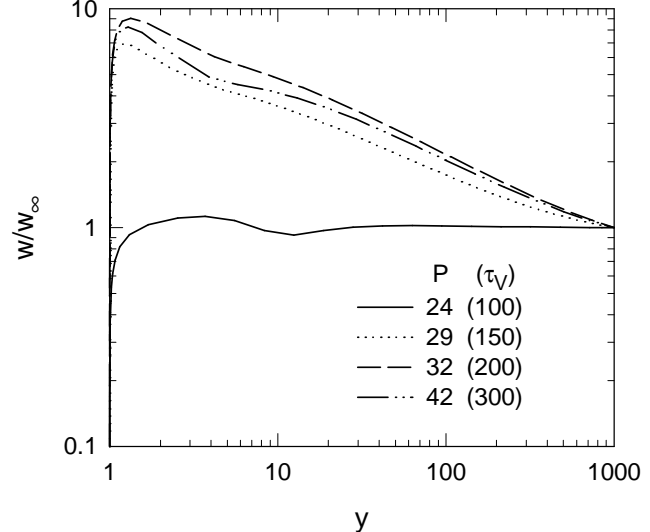


Figure 6. Gravitational quenching because of reddening. Models are for silicate dust with the listed values of P (the corresponding τ_V is in parenthesis). In each case θ and Γ are adjusted so that $w_\infty = 10\theta$ and the gravitational pull reaches 99% of its possible maximum; the detailed procedure is described in Appendix D.

Γ) or the reddening (smaller ϕ). The quenching process depends on all three input parameters and takes different forms in the optically thick and thin regimes. In optically thin winds $\phi = 1$ and since ζ increases monotonically with w (cf figure 2), the liftoff condition ensures positive acceleration everywhere. Consider the analytic solution (eq. 33) when δ increases while P and θ remain fixed. When $\beta = \delta/\delta_{\max}$ approaches unity the acceleration becomes negligible, though it remains positive, producing the behavior seen in the plots for $\beta = 0.999$ and 0.99999 in figure 1. This quenching effect is caused by the logarithmic term. Near $y = 1$ this term dominates and the velocity increases very slowly. At a distance y roughly proportional to $P^{-2}\theta^{3/2}|\ln(1-\beta)|$, the terms independent of δ take over and the acceleration picks up. From that point on the solution resembles non-quenched winds, albeit at a lower acceleration because of its late start. As β gets closer to unity, the dominance of the logarithmic term is slowly extended further out until the whole wind is stalled.

Reddening introduces an entirely different quenching mode, affecting winds that obey the liftoff condition when P is increased beyond a certain point. The liftoff condition ensures that the initial acceleration is always positive, irrespective of optical depth. However, subsequent reddening can reduce ϕ substantially (figure 2) and since the acceleration is proportional to $\phi \zeta - 1/\Gamma$, the wind may be prevented from reaching a significant terminal velocity. Furthermore, since $\phi \zeta < \phi$ the acceleration becomes negative whenever $\phi < 1/\Gamma$ and the velocity can even decline after its initial rise. Figure 6 shows examples of such winds whose velocity profile differs greatly from the monotonic rise that typifies all solutions not too close to the boundary of phase space. In each case $w_\infty = 10\theta$. But when $P \gtrsim 25$, the velocity reaches intermediate values substantially higher than w_∞ , almost as much as ten times higher, before declining to its final value. This behavior has intriguing observational impli-

cations, but it is not clear whether the limited phase space for such solutions affords a meaningful number of cases.

5.2 Phase Space Boundaries

Every point in the 3-dimensional P - Γ - θ space that results in a physical solution can be labeled by w_∞ of that solution. The equation $w_\infty(P, \Gamma, \theta) = C\theta$, where $C \geq 3$ is some prescribed number, defines a 2-dimensional surface in the solution space. This surface is the locus of solutions whose velocity increases by factor C , i.e., every wind on this surface has $v_\infty/v_T = C$. The volume enclosed by this surface corresponds to solutions with $v_\infty/v_T \geq C$, solutions outside this volume have $v_\infty/v_T < C$.

Figure 7 shows the projections onto the P - Γ plane of two such surfaces with representative values of v_∞/v_T . Each curve encloses the allowed region for winds whose v_∞/v_T is at least as large as the boundary mark. These boundaries are best understood by considering the wind problem at a fixed Γ . Moving from the bottom of the figure along a line of constant Γ and increasing P , the curve for a given v_∞/v_T is first intersected at its lower branch. This intersection defines a minimal P for physical solutions, which can be estimated by inserting θ from the liftoff condition into equation 62; a more accurate expression for this P_{\min} follows from the analytic solution for optically thin winds. The region below the lower branch is forbidden for that particular v_∞/v_T . Increasing P further crosses into the allowed region, leading to winds whose v_∞/v_T exceeds the boundary mark. Eventually, quenching by reddening sets a maximum to the value of P that still allows v_∞/v_T as large as the boundary mark. This P_{\max} corresponds to the second intersection with the curve, and the region above the upper branch again is forbidden. The two branches of each v_∞/v_T boundary are defined by the two gravitational quenching modes and reflect the central role of P in controlling both the dynamics and radiative transfer; this parameter sets the scales for both the acceleration (eq. 24) and optical depth (eq. 25). The physical domain for P is between the two branches, $P_{\min} < P < P_{\max}$. As Γ decreases, the gravitational force increases and the two branches approach each other: P_{\min} becomes larger (it takes stronger acceleration to overcome gravity) and P_{\max} becomes smaller (it takes less reddening to quench the wind). The meeting point of the two branches defines an absolute minimum for Γ , determined exclusively by the grain properties. Below this minimum, liftoff requires such a high P that reddening quenches the wind immediately. Note that this minimum is about 3–5 times larger than the Eddington limit $\Gamma = 1$, showing that the latter is not a sufficient condition for radiatively driven winds when the dust drift is taken into account (see below).

The plots in figure 7 outline the proper phase space boundaries for radiatively driven winds, replacing the erroneous bound $\dot{M}v_\infty \leq L/c$. If the velocity of a wind increases by a certain ratio, the parameters P and Γ of that wind necessarily lie inside the region bounded by the curve plotted for that ratio. The parameter θ is not shown in this projection but must conform to the bounds expressed by the liftoff condition and equation 62.

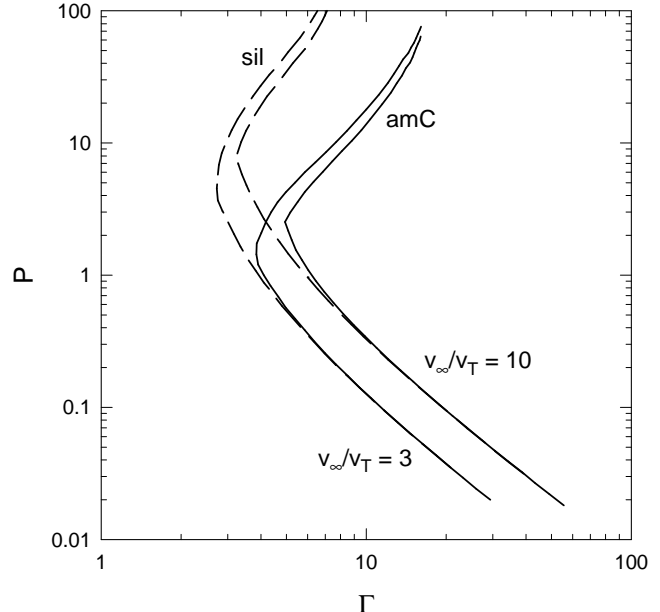


Figure 7. Phase space boundary: The parameters P and Γ of winds whose velocities increase by the indicated ratios v_∞/v_T must lie to the right of the correspondingly marked boundaries. The boundaries for amorphous carbon are marked by amC, for silicate grains by sil.

5.2.1 The Lower Branch; Minimal \dot{M}

This branch reflects the constraints imposed by equation 62 and the liftoff condition. Equation 62 implies that $w_\infty < P$ in all winds, namely $v < v_p$. As we discussed in §2, observations usually give $v \ll v_p$. While this inequality poses a problem for the simple GS solution, the proper inclusion of drift and reddening shows that it actually provides important support for radiation pressure as the driving mechanism in dusty winds.

From the liftoff condition (26), all winds must obey $\Gamma > 1$, the standard Eddington limit. Figure 7 shows that in dusty winds this bound is superseded by the combined effects of drift and reddening, which together impose a more stringent lower limit on Γ . The Eddington limit would be meaningful if the dust and gas were position coupled, instead the relevant regime in AGB winds is momentum coupling (see Gilman 1972). Indeed, $\Gamma > 1$ implies

$$\frac{L_4}{M_0} Q_* \sigma_{22} > 2.18 \times 10^{-2} \quad (63)$$

and this condition is obeyed by a large margin with typical parameters of observed winds. Although the Eddington limit does not impose a meaningful bound it provides another consistency check on the basic premises of the model.

The liftoff condition also implies that

$$\theta > \frac{1}{4} \left[\left(\frac{\Gamma + 3}{\Gamma - 1} \right)^{1/2} - 1 \right]^2 \simeq \begin{cases} (\Gamma - 1)^{-1} & \text{when } \Gamma \rightarrow 1 \\ \Gamma^{-2} & \text{when } \Gamma \gg 1 \end{cases} \quad (64)$$

Since Γ cannot approach unity (figure 7), the meaningful constraint is $\theta > \Gamma^{-2}$. From its definition in equation 23, $\theta = \dot{M}/\dot{M}_c$ where

$$\dot{M}_c = \frac{Q_* L}{v_{\text{TC}}} = 7.06 \times 10^{-5} \frac{Q_* L_4}{T_{\text{k3}}^{1/2}} \text{ M}_\odot \text{ yr}^{-1} \quad (65)$$

is a characteristic mass loss rate defined by the free parameters. Therefore, the liftoff condition implies a lower bound on the mass loss rate

$$\dot{M} > \frac{\dot{M}_c}{\Gamma^2}. \quad (66)$$

When this constraint is violated, the grains are ejected without dragging the gas because the density is too low for efficient momentum transfer from the dust to the gas.

The practical application of this result requires care. This constraint directly reflects our handling of the wind origin, the least understood part of the problem. Our liftoff condition is predicated on the assumption of positive acceleration right from the start. However, the initial acceleration in fact is negative in the two-fluid formulation that neglects gas pressure; starting such a calculation with $v = v_a$ produces a negative dv/dr , as is evident from both the NE (their equation 36) and HTT (eq. 7) studies. The wind is still lifted in these calculations because the dust accelerates, reversing the initial gas infall. But the negative derivative in turn reflects the shortcomings of these studies since the gas is in hydrostatic equilibrium in the absence of dust. This deficiency is removed in the study by Kwok (1975) which includes also gas pressure. At the sonic point Kwok finds $F_{\text{rad}}/F_{\text{grav}} < 1$ (his equation 15), in direct conflict with our liftoff assumption; the relation between the two forces is reversed only after further grain growth. But Kwok's result, too, is unrealistic because it neglects the effect of radiation pressure on the gas molecules, likely to be instrumental in initiating the outflow (e.g. Elitzur, Brown & Johnson 1989).

An exact calculation of the minimal \dot{M} is beyond the scope of our study. It would require proper inclusion of physical processes, such as grain growth, whose understanding is still rudimentary at best. It is also instructive to recall that even the formulation of drag is only accurate to within "... factors of order 2 or 3, which depend on accommodation coefficients and geometric factors" (Salpeter 1974). Fortunately, these uncertainties involve only the very initial stage of the outflow and the severity of their impact is greatly reduced once the flow settles into the highly supersonic stage that is the main thrust of our study. Indeed, the minimal dependence on θ of our final results demonstrates that for the most part, the initial conditions are quite irrelevant in the supersonic regime. While $\Gamma^2\theta > 1$ remains a strict requirement of our model, in reality this liftoff constraint could be less restrictive without an appreciable effect on most of our conclusions.

We propose a phenomenological substitute for the mathematical liftoff constraint

$$\Gamma^2\theta \gtrsim f, \quad (67)$$

where $f (< 1)$ is an unknown factor. This only affects results that directly involve the liftoff relation — the location of the lower branch of the phase-space boundary (figure 7) and the estimate of the lower bound on \dot{M} (equation 66). We estimate the phenomenological factor f by noting that it is mostly relevant at small P . In that region our solution gives $w_\infty^3 = \frac{9}{16}P^4$ (equation C4), which can be rewritten as

$$\Gamma^2\theta = \frac{16}{9} \left(\frac{v_{\text{T}}}{v_{\text{g}}} \right)^4 \left(\frac{v_\infty}{v_{\text{T}}} \right)^3. \quad (68)$$

With nominal values for v_{T} and v_{g} , the requirement $v_\infty/v_{\text{T}} \gtrsim 3$ and consistency of the last two relations set $f \sim 0.1$. As a result,

$$\dot{M} \gtrsim f \frac{\dot{M}_c}{\Gamma^2} \simeq 3 \times 10^{-9} \frac{M_0^2}{Q_* \sigma_{22}^2 L_4 T_{\text{k3}}^{1/2}} \text{ M}_\odot \text{ yr}^{-1} \quad (69)$$

replaces equation 66 as our phenomenological estimate of the minimal \dot{M} . It may be noted that HTT proposed a similar relation.

5.2.2 The Upper Branch; Maximal \dot{M}

The upper branch of the phase space boundary is defined by the quenching effect of reddening. Since it involves the wind outer regions where the supersonic flow is well established, it does not suffer from the liftoff uncertainties that afflict the lower branch. The upper branch defines a maximum \dot{M} when the other parameters are fixed, discussed in paper II.

6 GRAIN MIXTURES

We now discuss the general case of a mixture of grains that can have different sizes and chemical compositions. For the most part, the results of the single-type case hold. A new feature is the variation of the mixture composition because of different drift velocities.

The i -component of the mixture is defined by its grain size a_i and efficiency coefficients $Q_{i,\lambda}$; the latter may reflect differences in both size and chemical composition. As before, the details of production mechanism are ignored. We define the wind origin $y = 1$ as the point where the last grain type added to the mix enables the conditions for momentum coupling, initiating the supersonic gas outflow. We assume no further change in grain properties and denote the density of species i at that point $n_i(1)$ and its fractional abundance $x_{1i} = n_i(1)/n_d(1)$.

6.1 Scaling Formalism

In analogy with the single-type case, the reddening profile of the i -th species is

$$\phi_i(y) = \frac{1}{Q_{*,i}} \int Q_{\text{pr},i\lambda} \frac{F_\lambda(y)}{F(y)} d\lambda, \quad (70)$$

where

$$Q_{*,i} = \frac{\pi}{\sigma T_*^4} \int Q_{\text{pr},i\lambda} B_\lambda(T_*) d\lambda.$$

Since grain-grain collisions are negligible, different types of grains drift through the gas in response to the radiation pressure independent of each other. The velocity of species i is v_i and the ratio n_i/n_{H} varies in proportion to $\zeta_i(y) = v/v_i$. Introduce

$$q_i = \frac{Q_{*,i}}{Q_*}, \quad \text{where } Q_* = \sum_i x_{1i} Q_{*,i}. \quad (71)$$

With the aid of the mixture average Q_* we define v_m as before (equation 10), and the drift function of the i -th species is

$$\zeta_i(y) = \frac{\theta + \sqrt{wq_i\phi_i}}{\theta + q_i\phi_i + \sqrt{wq_i\phi_i}}, \quad (72)$$

where w and θ are the same as in the single-type case (eq. 23). The radiation pressure force per unit volume is

$$\mathcal{F}_{\text{rad}} = \frac{LQ_*}{4\pi r^2 c} \sum_i n_i(y) \pi a_i^2 q_i \phi_i(y). \quad (73)$$

We generalize the definition of cross-section area per gas particle (equation 5) via

$$f_i \sigma_g = \pi a_i^2 \frac{x_{1i}}{\zeta_i(1)} \frac{n_d(1)}{n_H(1)} \quad \text{and} \quad \sum f_i = 1, \quad (74)$$

so that f_i is the fractional contribution of species i to σ_g . At every point in the shell $n_i \pi a_i^2 = n_H \sigma_g f_i \zeta_i$ and the equation of motion is

$$\frac{dw^2}{dy} = \frac{P^2}{y^2} \left[\sum_i f_i q_i \phi_i(y) \zeta_i(y) - \frac{1}{\Gamma} \right] \quad (75)$$

where P and Γ are defined as before. The equation of motion retains its single-type form, the only modification is the weighted sum in the radiation pressure term. The dust properties require now a larger amount of input but the other parameters remain the same — P , θ and Γ .

The radiative transfer equation requires as input the overall optical depth τ_V and dust density profile η . Introduce the normalized density profile of the i -th species

$$\eta_i(y) = \frac{\zeta_i(y)}{y^2 w(y)} \left(\int_1^\infty \frac{\zeta_i}{y^2 w} dy \right)^{-1} \quad (76)$$

and the coefficients

$$z_i = Q_{Vi} f_i \int_1^\infty \frac{\zeta_i}{y^2 w} dy \quad (77)$$

where Q_{Vi} is the absorption efficiency at visual of the i -th species. Then

$$\eta = \frac{\sum_i z_i \eta_i}{\sum_i z_i}, \quad \tau_V = \frac{1}{2} P^2 \sum_i z_i \quad (78)$$

and the radiative transfer problem again does not require any additional input parameters. The most general dusty wind problem is fully prescribed by the grain properties and the three free parameters P , θ and Γ .

6.2 The Wind Velocity

The wind velocity profile remains similar to the single-type case. Consider first optically thin winds, where $\phi_i = 1$. An analytic solution does not exist now but the problem reverts to the single-grain case in two limits. When w is sufficiently small that $w < q_i$ for every i , drift dominates all grain types and the $k = \frac{2}{3}$ profile of eq. 35 is recovered. In the opposite limit of $w > q_i$ for every i , drift is negligible for all grains and eq. 35 again applies with $k = \frac{1}{2}$. In reality, the grain types are distributed between these two extremes. Different types move from the drift-dominated to the negligible-drift regimes as w increases, and the gas velocity profile evolves slowly from one shape to the other. Since the two profiles

are quite similar, the overall behavior does not differ significantly from the single-grain case. And since the only effect of reddening is to decrease k slightly further, the qualitative similarity remains for optically thick winds.

6.3 Radial Variation of Grain Abundances

Grains of different types have different velocities, creating a radial variation of the fractional abundances. The final abundance of species i is $x_{1i} E_i / E$ where

$$E_i = \frac{\zeta_i(\infty)}{\zeta_i(1)} \quad (79)$$

and $E = \sum x_{1i} E_i$. Since ζ is monotonically increasing, $E_i > 1$ for every grain type and $E > 1$. The outflow enhances the overall dust abundance, the final value of n_d/n_H always exceeds its initial value. The fractional abundance is enhanced for grains with $E_i > E$ and suppressed for those with $E_i < E$.

For simplicity, we discuss the behavior of this differential enhancement only in the optically thin limit ($\phi_i = 1$), where E_i has the approximate behavior

$$E_i \simeq \begin{cases} 1 & q_i < \theta \\ \left(\frac{q_i}{\theta}\right)^{1/2} & \theta < q_i < w_\infty \\ \left(\frac{w_\infty}{\theta}\right)^{1/2} & w_\infty < q_i \end{cases} \quad (80)$$

This result is easy to understand. At a position where the gas velocity is w , grains with $q_i < w$ maintain a constant ratio v_i/v and have $\zeta_i = 1$. Those with $q_i > w$ are falling behind and have $\zeta = (w/q_i)^{1/2}$. The expression for E_i reflects the two limiting cases of grains that are either moving with the gas ($q_i < \theta$) or lagging behind ($q_i > w_\infty$) throughout the entire outflow, and the intermediate case of grains that are falling behind until the wind has accelerated to the point that $w = q_i$.

The differential enhancement is controlled by q_i , the ratio of Q_* for the particular grain type and for the whole mixture. The dependence of this quantity on grain size can be derived in a simple model that ignores spectral features, approximating the efficiency coefficient with

$$Q(\lambda, a) \simeq \begin{cases} 1 & \lambda < 2\pi a \\ \left(\frac{2\pi a}{\lambda}\right)^\beta & \lambda > 2\pi a \end{cases} \quad (81)$$

This crude approximation, with $\beta \sim 1-2$, is adequate for most purposes. Approximating the spectral averaging in the definition of Q_* with its value at the peak wavelength of the Planck distribution produces

$$Q_*(a) \simeq \begin{cases} 1 & a > a_* \\ \left(\frac{a}{a_*}\right)^\beta & a < a_* \end{cases} \quad (82)$$

where $a_* = 0.64 \mu\text{m}$ ($1000 \text{ K}/T_*$). It is interesting to note that $T_* = 2500 \text{ K}$ gives $a_* = 0.25 \mu\text{m}$, same as the upper bound of the MRN grain size distribution (Mathis, Rumpl & Nordsieck 1977).

Consider an initial power-law grain size distribution of the form

$$n_d(a, y=1) \propto a^{-p} \quad \text{for} \quad a_{\min} \leq a \leq a_* \quad (83)$$

defined by the free parameters p and a_{\min} (the MRN distribution corresponds to the special case with $p = 3.5$ and $a_{\min} = 0.005 \mu\text{m}$). With this general form,

$$q(a) = \left(\frac{a}{a_1}\right)^\beta, \quad \text{where } a_1 = a_{\min} \left(\frac{p-1}{p-\beta-1}\right)^{1/\beta}. \quad (84)$$

Only the lower bound a_{\min} enters here, $q(a)$ is independent of the upper bound a_* . The result for the abundance enhancement factor is

$$E(a) \simeq \begin{cases} 1 & a < a_1 \theta^{1/\beta} \\ \left(\frac{a}{a_1 \theta^{1/\beta}}\right)^{\beta/2} & a_1 \theta^{1/\beta} < a < a_1 w_\infty^{1/\beta} \\ \left(\frac{w_\infty}{\theta}\right)^{1/2} & a_1 w_\infty^{1/\beta} < a \end{cases} \quad (85)$$

The drift enhances preferentially the upper end of the size distribution, grains smaller than a certain size do not drift at all and their abundance is never enhanced. *A power-law distribution that starts with index p emerges as a power-law distribution with the reduced index $p - \beta/2$.* To produce the MRN index of 3.5, the size distribution must start with a higher index of $\sim 4\text{--}4.5$.

A complete theory for the grain distribution cannot be constructed without including the details of the production process. Our results show that some properties of the MRN distribution are natural features in the subsequent effect the outflow has on the fractional abundances. It is possible that the MRN distribution could emerge as the only self-consistent solution of the complete theory.

7 SUMMARY AND DISCUSSION

Given grain properties, we have shown here that the supersonic phase of dusty winds is specified in terms of three independent dimensionless variables. A bank of solutions derived in the 3-dimensional space of these variables will contain the dimensionless density and velocity profiles of any possible wind around an evolved star. Matching the complete observations of any particular system requires at most scaling by an overall velocity scale. In addition, the solution of the radiative transfer problem is also contained in the outcome. We find that the solutions are generally controlled by a single parameter and can be described in terms of self-similarity functions that are independent of grain properties. Therefore, the results presented here contain the solution for the dynamics problem for all grains. The corresponding spectral energy distributions were presented elsewhere for amorphous carbon and silicate dust (IE95, IE97). Thanks to scaling, extending that database to any other grain composition is as simple as a single run of DUSTY in which τ_V is varied over its entire feasible range.

Our formulation starts once the dust properties are established. These properties, as well as the value of \dot{M} , are set during an earlier phase of the outflow. This initial phase is still poorly understood and our analysis has nothing to say about it. However, most observations involve the subsequent supersonic phase, which is the one addressed here. We associate the starting radius r_1 with prompt dust formation, but this does not enter directly into the solution because r_1 drops out of our formulation. Extended, rather

than prompt, dust formation can be accommodated without any change if r_1 is identified with the endpoint of grain growth. The association of r_1 with dust condensation enters only indirectly—since the region $r < r_1$ is devoid of dust, the diffuse radiation vanishes at r_1 (IE97). Even this indirect effect is inconsequential in optically thin systems, where the dynamics impact of the diffuse radiation is negligible altogether. Therefore, *our analytic solution eq. 33 is valid in all optically thin winds irrespective of the nature of dust formation*; if grain growth is extended over a distance comparable with the dynamics length scale, the solution simply becomes applicable from the point where that growth stops. The only direct reference to the association of dust condensation with r_1 occurs when this radius is expressed in terms of other physical quantities (eq. 40). If the explicit dependence on r_1 is instead left intact, any arbitrary model of dust condensation can be incorporated through the behavior it gives for r_1 . Young's correlation (sec. 4.2) implies that $r_1 \propto L^{1/2}$, consistent with prompt dust formation.

One of the grain parameters employed here is the cross-section area per hydrogen nucleus σ_g . This quantity is directly related to the ratio of dust-to-gas mass loss rates

$$r_{dg} = \frac{\dot{M}_d}{\dot{M}} = \frac{4\rho_s}{3m_p} a \sigma_g \quad (86)$$

where ρ_s is the density of the dust solid material. This ratio (which requires additionally ρ_s) was used as an input in the calculations of HTT, who denoted it δ and pointed out its significance to the wind solution. Our analysis shows that σ_g actually does not enter into the scaling formulation of the problem; indeed, we have solved here the dusty wind problem for two different types of grains without ever specifying the value of σ_g for either of them. The only dust properties required are the efficiency coefficients Q_λ and sublimation temperature T_c . Even the grain size is not strictly needed since it only enters indirectly as one factor, albeit a major one, in determining Q_λ . The dust abundance is an extraneous parameter controlling only the correspondence between the model results and physical quantities, just like the velocity scale which is irrelevant for the solution itself.

Our analysis highlights the central roles that drift and reddening play in the velocity structure of dusty winds. Independent of grain properties, the significance of drift is diminished when $P > \frac{16}{9}$, a universal result reflecting the mathematical structure of the equation of motion. Reddening, on the other hand, becomes important at $\tau_V > 1$ and the corresponding P is determined by Q_V (equation 37). If Q_V were, say, 10^{-2} reddening would start playing a role only at $P > 100$, long after the drift ceased to be a factor. Since astronomical dust has Q_V of order unity, reddening starts controlling the force just as the drift dominance ends.

Finally, why are typical velocities of AGB winds $\sim 10\text{--}20 \text{ km s}^{-1}$? Our results provide explanations for both the magnitude and the narrow range of v_∞ . While the driving force is radiation pressure, drift and reddening play a fundamental role. Rapid drift at small τ_V decreases the dust abundance from its initial value, reducing the captured fraction of radiative energy. And at large optical depths this fraction is similarly reduced because the radiation spectral shape is shifted toward longer wavelengths where the absorption efficiency is small. The two effects combine to produce the very narrow range of velocities displayed by equation 53

— the range of variation with either L or τ_V is less than factor of 3, the dependence on dust properties is similarly weak. Given that the luminosity scale is $\sim 10^4 L_\odot$, the velocity magnitude is determined by the dust parameters. Single grain properties cannot deviate much from the values listed in Table 1, the only parameter that is completely free is the dust abundance. Since the velocities are typically $\sim 10 \text{ km s}^{-1}$, the dust abundance must be such that σ_{22} is of order unity; were that abundance 100 times higher, typical velocities would be $\sim 100 \text{ km s}^{-1}$ instead. This implies that the dust is produced with an abundance comparable to that found in the general interstellar medium and resolves the conflicts pointed out by Castor (1981).

ACKNOWLEDGMENTS

We thank Haggai Elitzur for instrumental advice on the analytic solution of optically thin winds. The partial support of NASA and NSF is gratefully acknowledged.

REFERENCES

Bowen, G.H. 1989, in *Evolution of peculiar red giant stars*, ed. H.R. Johnson & B. Zuckerman (Cambridge University Press: Cambridge), p. 269

Castor, J.I. 1981, in *Physical Processes in red Giants*, eds. I. Iben & A. Renzini (Reidel: Dordrecht), p. 285

Elitzur, M., Brown, J.A. & Johnson, H.R., 1989, ApJ, 341, L95

Fleischer, A.J., Winters, J.M., & Sedlmayr E. 1999, in *AGB Stars*, ed. Le Bertre, T., Lébre, A., & Waelkens, C. (ASP: San Francisco), p. 187

Gilman, R.C. 1972, ApJ, 178, 423

Goldreich, P., & Scoville, N., 1976, ApJ, 205, 144 (GS)

Habing, H.J., Tignon, J. & Tielens, A.G.G.M. 1994, A&A 286, 523 (HTT)

Hanner, M.S. 1988, NASA Conf. Pub. 3004, 22

Höfner, S. 1999, in *AGB Stars*, eds. Le Bertre, T., Lébre, A., & Waelkens, C. (ASP: San Francisco), p. 159

Ivezić Ž., & Elitzur M., 1995, ApJ, 445, 415 (IE95)

Ivezić Ž., & Elitzur M., 1997, MNRAS, 287, 799 (IE97)

Ivezić Ž., & Elitzur M., 2001, in preparation (paper II)

Ivezić, Ž., Nenkova, M., Elitzur, M., 1999, User Manual for DUSTY, University of Kentucky Internal Report, accessible at <http://www.pa.uky.edu/~moshe/dusty>

Jura, M., 1984, ApJ 282, 200

Jura, M., 1991, A&A Rev. 2, 227

Knapp, G.P., Gunn, J.R. & Wynn-Williams, C.G., 1992, ApJ, 399, 76

Knapp, G.R., Young, K., Lee, E., Jorissen, A. 1998, ApJS, 117, 209

Kwok, S., 1975, ApJ, 198, 583

Mathis J.S., Rumpl W. & Nordsieck K.H. 1977, ApJ, 217, 425

Netzer N., & Elitzur M., 1993, ApJ, 410, 701 (NE)

Ossenkopf, V., Henning, Th. & Mathis, J.S. 1992, A&A, 261, 567

Salpeter, E.E., 1974, ApJ, 193, 579

Young, K. 1995, ApJ, 445, 872

APPENDIX A: GLOSSARY

a	dust grain radius	$K_1 \dots K_4$	similarity functions summarizing the solution observable implications (equations 48, 49 and 50)
E_i	abundance enhancement of the i -th component of a mixture owing to differential drift velocities (eq. 79)	L, L_4	luminosity and its magnitude in $10^4 L_\odot$
		M, M_0	stellar mass and its magnitude in M_\odot
		\dot{M}, \dot{M}_{-6}	mass loss rate and its magnitude in $10^{-6} M_\odot \text{ yr}^{-1}$
		n_d, n_H	number densities of dust grains and hydrogen nuclei, respectively
		$P = v_p/v_m$	main scaling parameter of the dimensionless equation of motion; sets the ratio of radiation pressure to the drift effect
		Q_V	the dust absorption efficiency at visual
		Q_*	Planck average at the stellar temperature of the efficiency coefficient for radiation pressure (eq. 4)
		q_i	fractional contribution of the i -th component of a mixture to Q_* (eq. 71)
		$r_1, r_{1,14}$	the wind inner radius and its magnitude in 10^{14} cm
		T_*	stellar temperature
		T_c, T_{c3}	the dust temperature at r_1 and its magnitude in 1,000 K
		T_k, T_{k3}	the kinetic temperature at r_1 and its magnitude in 1,000 K
		v, v_d, v_{rel}	velocities of the gas, dust and their difference, respectively
		v_p, v_m, v_g	velocity scales characterizing the radiation pressure (eq. 6), drift (10) and gravity (14), respectively
		v_T	the wind initial velocity (identified with the isothermal sound speed at r_1 ; eq. 9)
		v_∞, v_1	the wind final velocity and its magnitude in km s^{-1}
		$w = v/v_m$	dimensionless velocity
		$w_\infty = v_\infty/v_m$	the dimensionless final velocity
		$y = r/r_1$	dimensionless radial distance
		Γ	ratio of radiation pressure to gravity (eq. 15)
		$\delta = 1/(\Gamma - 1)$	auxiliary quantity for the analytic solution of optically thin winds
		$\zeta = v/v_d$	dimensionless drift profile (eq. 12)
		ζ_i	dimensionless drift profile of the i -th component of a gas mixture (eq. 72)
		η	dimensionless dust density profile (eq. 18)
		$\theta = v_T/v_m$	the dimensionless initial velocity
		Θ	the transformation function between P and τ_V (eq. 46)
		σ_g, σ_{22}	dust cross-section area per particle at condensation and its magnitude in 10^{-22} cm^2 (eq. 5)
		τ_V	overall optical depth at visual
		ϕ	reddening profile (eq. 3)
		Φ	velocity-weighted harmonic average of ϕ (eq. 27)
		$\bar{\phi}$	density-weighted average of ϕ (eq. 42)
		Ψ, Ψ_0	a dimensionless function determined by radiative transfer and its value in optically thin winds (eqs. 40 and 41)

APPENDIX B: DRIFT VELOCITY

The drag force on a grain moving at velocity v_{rel} through gas with density ρ is

$$F_{\text{drag}} = \pi a^2 \rho \times \begin{cases} v_{\text{rel}}^2 & \text{when } v_{\text{rel}} > v_T \\ v_{\text{rel}} v_T & \text{when } v_{\text{rel}} < v_T \end{cases} \quad (\text{B1})$$

for the subsonic ($v_{\text{rel}} < v_T$) and supersonic ($v_{\text{rel}} > v_T$) regimes (e.g., Kwok 1975). The drift reaches steady state when $F_{\text{drag}} = F_{\text{pr}}$, the radiation pressure force on the grain. Introduce

$$v_D^2 = \frac{F_{\text{pr}}}{\pi a^2 \rho} = \frac{1}{c\rho} \int Q_{\text{pr},\lambda} F_\lambda d\lambda, \quad (\text{B2})$$

then the steady-state drift velocity is

$$v_{\text{rel}} = \begin{cases} v_D & \text{when } v_D > v_T \\ \frac{v_D^2}{v_T} & \text{when } v_D < v_T \end{cases} \quad (\text{B3})$$

Both limits can be combined in the simple expression

$$v_{\text{rel}} = \frac{v_D^2}{v_D + v_T}. \quad (\text{B4})$$

Kwok proposed instead the more complex expression

$$v_{\text{rel}} = \left\{ \frac{1}{2} \left[(4v_D^4 + v_T^4)^{1/2} - v_T^2 \right] \right\}^{1/2}. \quad (\text{B5})$$

He derived this result by combining first into a single expression the two limiting forms of the drag force, instead of v_{rel} itself, and then solved the resulting quadratic equation for v_{rel} . Kwok's expression and ours are based on the same ingredients and give identical results in the limits of both $v_D > v_T$ and $v_D < v_T$.

APPENDIX C: ANALYTIC APPROXIMATIONS

The quantities of interest obtained from the solution of the equation of motion are the profile shapes of the velocity and density variation, the final velocity w_∞ and the optical depth τ_V . Introduce

$$u = \frac{w}{w_\infty}, \quad \epsilon = \frac{\theta}{w_\infty}, \quad \beta = \frac{\delta}{\delta_{\text{max}}}. \quad (\text{C1})$$

The profile shape is conveniently expressed in terms of u , which varies from ϵ to 1, with ϵ ($\leq \frac{1}{3}$) and β (< 1) as small parameters. Furthermore, we note that θ , too, is a small parameter in all practical cases and use $\delta_{\text{max}} = \theta + \sqrt{\theta} \simeq \sqrt{\theta}$ as well as $\delta - \theta \simeq \beta\sqrt{\theta}$.

C1 Negligible Reddening

When $\phi = 1$, the complete solution (eq. 33) gives the following equation for w_∞ :

$$\begin{aligned} P^2 &= w_\infty^2 (1 - \epsilon^2) (1 + \beta \epsilon^{1/2} w_\infty^{1/2}) \\ &+ \frac{4}{3} w_\infty^{3/2} (1 + \beta \epsilon^{1/2} w_\infty^{1/2})^2 \times \\ &\left[1 + \frac{3}{2} \beta \epsilon^{1/2} - 3 \beta^2 \epsilon - \epsilon^{3/2} (1 + \frac{3}{2} \beta + 3 \beta^2) \right. \\ &\left. + 3 \beta^3 \epsilon^{3/2} \ln \frac{1 - \beta \epsilon^{1/2}}{\epsilon^{1/2} (1 - \beta)} \right]. \end{aligned} \quad (\text{C2})$$

This expression is an expansion in the problem's small parameters. Consider first the limit $\beta = 0$, which gives

$$P^2 = \frac{4}{3} w_\infty^{3/2} (1 - \epsilon^{3/2}) + w_\infty^2 (1 - \epsilon^2). \quad (\text{C3})$$

At small values of w_∞ the first term on the right dominates, at large values the second. Keeping only the dominant term produces $w_\infty = (\frac{9}{16} P^4)^{1/3} (1 - \epsilon^{3/2})^{-2/3}$ in the first regime, $w_\infty = P (1 - \epsilon^2)^{-1/2}$ in the second. Neglecting the ϵ corrections, the two terms and the approximate solutions they yield are equal to each other at $w_\infty = P = \frac{16}{9}$. Since small w_∞ ensures $w < 1$ for the entire wind, $\zeta = w^{1/2}$ in that case while $\zeta = 1$ for most of the wind when $w_\infty \gg 1$ (see equation 24). Therefore, $P = \frac{16}{9}$ is the transition between drift dominance and negligible drift, and

$$w_\infty = \begin{cases} \left(\frac{9}{16} P^4 \right)^{1/3} & \text{for } P < 16/9 \text{ (drift dominated)} \\ P & \text{for } P > 16/9 \text{ (negligible drift)} \end{cases} \quad (\text{C4})$$

These two limit expressions for w_∞ can be combined in the single form listed in equation 36.

Finite β corrections are generally small when $\epsilon \leq \frac{1}{3}$ and $\beta \leq \frac{1}{2}$. The deviations from unity of the terms inside the large square brackets are less than 30% in that domain. The only significant corrections can come from the terms in $\beta \epsilon^{1/2} w_\infty^{1/2}$. Since $w_\infty \leq P$, $\beta \epsilon^{1/2} w_\infty^{1/2} < 0.3 P^{1/2}$ for all $\epsilon \leq \frac{1}{3}$ and $\beta \leq \frac{1}{2}$. Therefore, this term is always negligible in the drift dominated regime. But at large P it can become significant, at $P = 10$ it already amounts to a 90% correction. When this term dominates, the solution becomes $w_\infty^5 = P^4 / \beta^2 \epsilon$. However, reddening effects become significant before this limit is reached, therefore we are justified in maintaining the $\beta = 0$ approximation; figure 1 shows that this faithfully presents the entire $\epsilon \leq \frac{1}{3}$ and $\beta \leq \frac{1}{2}$ domain.

We proceed now to the velocity profile. With $\beta = 0$, equation 33 gives

$$\frac{u^2 - \epsilon^2 + \frac{4}{3} w_\infty^{-1/2} (u^{3/2} - \epsilon^{3/2})}{1 - \epsilon^2 + \frac{4}{3} w_\infty^{-1/2} (1 - \epsilon^{3/2})} = 1 - \frac{1}{y}. \quad (\text{C5})$$

Similar to equation C3, this equation changes its behavior at $w_\infty = \frac{16}{9}$; at smaller w_∞ the terms proportional to $\frac{4}{3} w_\infty^{-1/2}$ dominate, at larger w_∞ the other terms. The two limits give

$$u = \left(1 - \frac{1 - \epsilon^{1/k}}{y} \right)^k, \quad k = \begin{cases} 2/3 & \text{for } P < 16/9 \\ 1/2 & \text{for } P > 16/9 \end{cases} \quad (\text{C6})$$

From this we can immediately determine the dust density normalized profile η ($\propto \zeta/y^2 u$), required for the radiative transfer equation. The ratio ζ/u is proportional to $1/u^{1/2}$ in the drift-dominated regime and to $1/u$ when the drift is negligible. With the particular value for k in each case, ζ/u is the same as $1/u$ with the power index $-k$ replaced by $1 - k$, leading to

$$\eta = \frac{A}{y^2} \left(\frac{y}{y - 1 + \epsilon^{1/k}} \right)^{1-k}, \quad A = k \frac{1 - \epsilon^{1/k}}{1 - \epsilon}. \quad (\text{C7})$$

The velocity and density profiles are independent of P , which is relevant only for the choice of the solution regime. The only parameter that enters explicitly is ϵ , and even this dependence is confined mostly to the wind origin where $u(1) = \epsilon$ and $\eta(1) = A/\epsilon^{(1-k)/k}$. However, the ϵ -dependence,

which must be maintained to avoid a singularity for η at $y = 1$, rapidly disappears once $y > 1 + \epsilon$.

C2 Reddening Corrections

Reddening corrections are conveniently expressed in terms of the quantity Φ . Since ϕ decreases away from the wind origin, the averaging is dominated by its upper end and

$$\Phi \simeq \frac{\phi(y \rightarrow \infty)}{1 - \epsilon}. \quad (\text{C8})$$

For simplicity, only $\delta = 0$ is considered. The equivalent of equation C3 is then

$$P^2 = \frac{4}{3} w_\infty^{3/2} \int_\epsilon^1 \frac{du}{\sqrt{\phi}} + w_\infty^2 \int_\epsilon^1 \frac{du}{\phi}. \quad (\text{C9})$$

Approximating the integrand in the first term by its largest value, our approximate solution for w_∞ becomes

$$P^2 = \frac{4w_\infty^{3/2}}{3\sqrt{\Phi}} + \frac{w_\infty^2}{\Phi}. \quad (\text{C10})$$

In analogy with equation C3 this yields

$$w_\infty = \begin{cases} \left(\frac{9}{16}P^4\Phi\right)^{1/3} & \text{for } P < \frac{16}{9}\Phi^{1/2} \\ P\Phi^{1/2} & \text{for } P > \frac{16}{9}\Phi^{1/2} \end{cases} \quad (\text{C11})$$

C3 Optical Depth

The relation between P and τ_V is obtained by combining equations 28 and C10. When $\delta = 0$,

$$\frac{P^2}{\Phi} = \frac{4}{3} \left(\frac{\tau_V}{Q_V} \right)^{3/2} + \left(\frac{\tau_V}{Q_V} \right)^2. \quad (\text{C12})$$

From this we can find the value of P that yields $\tau_V = 1$. With the approximation $\Phi \simeq 1$ at this point we get

$$P = \frac{1}{Q_V} \left(1 + \frac{4}{3} Q_V^{1/2} \right)^{1/2}. \quad (\text{C13})$$

Finally, the δ -dependent correction term in equation 28 can be estimated in the optically thin case. With the leading-order velocity profile from equation C6, the integration result is

$$\int_1^\infty \frac{dy}{y^2 u} = \frac{1}{1 - k} \frac{1 - \epsilon^{(1-k)/k}}{1 - \epsilon^{1/k}}. \quad (\text{C14})$$

APPENDIX D: NUMERICAL PROCEDURES

The velocity and density profiles are very steep near the wind origin (cf eq. C7). As a result, the solution of the equation of motion 24 can become a difficult numerical problem that requires a prohibitive number of radial grid points, especially when optical depths are large. To bypass these problems, we find the velocity profile instead from the integral equation expressed by the formal solution

$$w^2 = \theta^2 + P^2 \left[z(y) - \frac{1}{\Gamma} \left(1 - \frac{1}{y} \right) \right], \quad (\text{D1})$$

where

$$z = \int_1^y \phi \zeta \frac{dy}{y^2}. \quad (\text{D2})$$

Given ϕ , this equation is solved by iterations that start with the analytic solution for w derived in the previous section.

The code DUSTY (Ivezić et al, 1999) starts by solving the radiative transfer equation with an initial density profile η taken from equation C7. The resulting reddening profile ϕ is used in equation D1 to find w . A new reddening profile is calculated with the corresponding η (see equation 25), and the process is repeated until ϕ , η and w are self-consistent. Convergence is rapid and the number of radial grid points is modest — less than 30 points are adequate for optical depths up to 100. The power of the method stems from the fact that the steepness of the velocity and density profiles is built in right from the start.

We find it advantageous to replace P , Γ and θ with three other independent input parameters. First, because of the central role of radiative transfer we specify the optical depth τ_V and determine P from

$$P^2 = \frac{2}{N} \frac{\tau_V}{Q_V}, \quad \text{where } N = \int_1^\infty \frac{\zeta}{y^2 w} dy \quad (\text{D3})$$

(see equation 25). Next, consider the quantity

$$g_{\max} = \max \frac{1 - \frac{1}{y}}{z(y)}, \quad (\text{D4})$$

the maximum of the prescribed profile anywhere in the shell. The wind stalls when $g_{\max} = \Gamma$, therefore physical solutions have $g_{\max} = f\Gamma$ with $f < 1$. We choose f as an input parameter instead of Γ with the replacement

$$\frac{1}{\Gamma} = \frac{f}{g_{\max}}. \quad (\text{D5})$$

The parameter f varies from 0 for negligible gravity to 1 for gravitationally quenched winds. Finally, instead of θ we specify as an input parameter $\epsilon = \theta/w_\infty$. If Y denotes the shell outer radius, θ is derived from the formal solution at that point, which gives

$$\theta^2 = \frac{\epsilon^2}{1 - \epsilon^2} P^2 \left[z(Y) - \frac{1}{\Gamma} \left(1 - \frac{1}{Y} \right) \right]. \quad (\text{D6})$$

The advantage of τ_V , ϵ and f over P , θ and Γ as input parameters is the more direct contact they have with physical quantities. In particular, the choice $\epsilon \leq \frac{1}{3}$ and $f < 1$ guarantees a priori a physically meaningful solution.